Evaluation of DC Resistivity and Time-Domain IP Tomography for Bedrock Characterisation at Önneslöv, Southern Sweden

Daniel Preis Bergdahl

Dissertations in Geology at Lund University,
Master's thesis, no 492
(45 hp/ECTS credits)

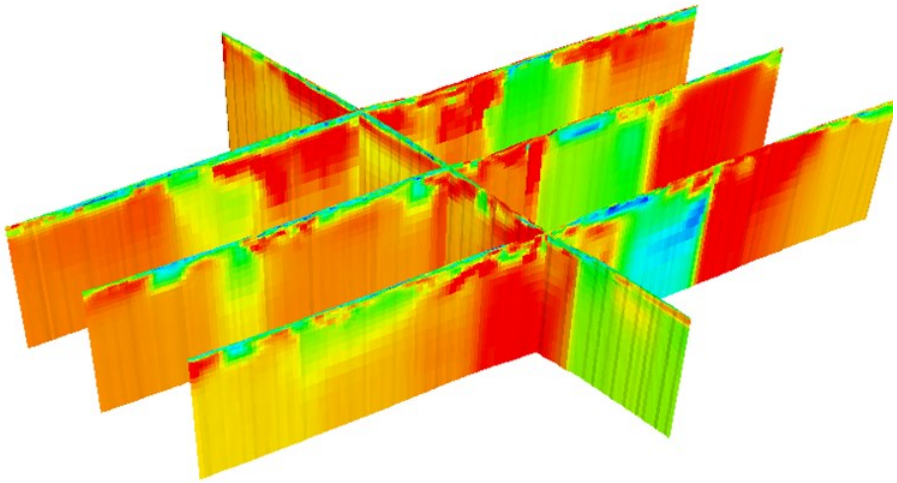

Department of Geology
Lund University
2016

Evaluation of DC Resistivity and Time-Domain IP Tomography for Bedrock Characterisation at Önneslöv, Southern Sweden

Master's thesis

Daniel Preis Bergdahl

Department of Geology
Lund University
2016

Contents

Cover Picture: Inverted resistivity profiles from the study area at Önneslöv

Evaluation of DC Resistivity and Time-Domain IP Tomography for Bedrock Characterisation at Önneslöv, Southern Sweden

Daniel Preis Bergdahl

Preis Bergdahl, D., 2016: Evaluation of DC Resistivity and Time-Domain IP Tomography for Bedrock Characterisation at Önneslöv, Southern Sweden. *Dissertations in Geology at Lund University*, No. 492, 46 pp. 45 hp (45 ECTS credits).

Abstract: For both construction and exploration purposes, knowledge of the subsurface is important. Geophysical exploration methods can be used to acquire an overview of an area on which further investigations can be based. In this study direct current resistivity and induced polarization data, inverted with a Cole-Cole model in program AarhusInv, are used to characterize the bedrock at Önneslöv in Scania, southwestern Sweden. Önneslöv is situated at the Romele horst, which contain gneissic bedrock intruded by dykes.

Resistivity ρ, with the unit Ωm, is a measurement of a materials' resistance to electric current. Induced Polarization, IP, which is measured as chargeability *m* with the unit mV/V, is the materials ability to charge up as a capacitor due to displacement of charges. Since both are physical properties of a material they can be used to investigate the material in the ground. The Cole-Cole model calculates the chargeability when the charging current was cut m_0, as well as the frequency factor *C* and time constant τ. In contrast, commonly integral chargeability *m* is used, which uses a certain timeframe of the polarization decay. Magnetometry, percussion drillings, and borehole geophysics are also used to help refine and verify interpretations.

The results show several NW trending linear elements in the ground. Many of them are interpreted as dykes or weakness zones. Weathering zones and weathered bedrock surfaces are also possible to identify, especially when adding normalised IP. The ground also contains numerous NE trending deformed and metamorphosed dykes that cannot be seen directly in the resistivity and IP data. However, these dykes most likely contribute to generally low resistivity values for bedrock in the area. *C* and τ follow the IP in terms of magnitude and are believed to be connected to textural differences in the ground. An additional finding is that the colour of the gneissic bedrock corresponds with changes in the gamma ray borehole logs, most likely due to the amount of potassium bearing minerals.

Keywords: Resistivity, Induced Polarization, Cole-Cole, Bedrock, Dyke, Weathering.

Supervisor(s): Department of Geology: Ulf Söderlund

Engineering Geology: Torleif Dahlin, Sara Johansson, Per-Ivar Olsson, Matteo Rossi

Subject: Bedrock Geology, Applied Geology

Daniel Preis Bergdahl, Department of Geology, Lund University, Sölvegatan 12, SE-223 62 Lund, Sweden. E-mail: daniel_preis@hotmail.com

Utvärdering av direktströmsresistivitet och tids-domän inducerad polarisation tomografi för berggrundskarakterisering vid Önneslöv, Södra Sverige

Daniel Preis Bergdahl

Preis Bergdahl, D., 2016: Utvärdering av direktströmsresistivitet och inducerad polarization i tids-domän för berggrundskarakterisering vid Önneslöv, Södra Sverige. *Examensarbeten i geologi vid Lunds universitet*, Nr. 492, 46 sid. 45 hp.

Sammanfattning: Kunskap om markens uppbyggnad är viktig både för konstruktions och prospekteringsändamål. Geofysiska undersökningsmetoder kan användas för att skapa en överblick att basera vidare undersökningar på. I den här studien används likströms resistivitet och inducerad polarisation, IP. Datan är inverterad med en Cole-Cole modell i programmet ÅrhusInv och använd för att karakterisera berggrunden vid Önneslöv i Skåne. Önneslöv är beläget på Romele horsten som består av gnejs innehållande mafiska gångbergarter.

Resistivitet ρ, med enheten Ωm, är ett värde på ett materials resistans mot elektrisk ström. Inducerad polarisation, vilket mäts i uppladdningsförmåga *m* med enheten mV/V, är materialets förmåga att laddas som en kapacitator till följd av omfördelning av laddningar i marken. Eftersom de är fysiska egenskaper hos ett material kan de användas för att undersöka materialen marken. Cole-Cole modellen beräknar uppladdningseffekten vid tillfället då strömmen bröts m_0 samt frekvensfaktorn C och tidskonstanten τ. Detta skiljer sig från den vanligt förekommande integrerade inducerade polarisationen m, då den integrerar ett specifikt tidsavsnitt av urladdningen istället. Magnetometri, hammarborrningar och borrhålsgeofysik har även använts för att förbättra och verifiera tolkningar.

Resultaten visar flera NV gående linjära strukturer. Flera av dem är tolkade som gångbergarter och/eller svaghetszoner. Vittringszoner och vittrade delar av bergöverytan går även att identifiera, särskilt då normaliserad IP även används. Marken innehåller även ett stort antal mindre NO gående deformerade och metamorfoserade gångbergarter som inte går att se tydligt i resistivitets och IP datan. De bidrar dock troligtvis till generellt lägre resistivitetsvärden för berggrund i området. C och τ tycks följa IP värdena vad gäller högre eller lägre och tros bero på textuella skillnader i marken. Ett sidoresultat i den här studien är att färgen på gnejsen går att korrelera med variationen av gammastrålning i borrhålen, troligtvis beroende på mängden kaliuminnehållande mineral.

Nyckelord: Resistivitet, inducerad polarisation, Cole-Cole, berggrund, gångbergart, vittring.

Handledare: Geologiska institutionen: Ulf Söderlund,

Teknisk geologi: Torleif Dahlin, Sara Johansson, Per-Ivar Olsson, Matteo Rossi

Ämnesinriktning: Berggrundsgeologi, tillämpad geologi

Daniel Preis Bergdahl, Geologiska institutionen, Lunds Universitet, Sölvegatan 12, 223 62 Lund, Sverige. E-post: daniel_preis@hotmail.com

1 Introduction and Aim

Knowing the characteristics of the bedrock is important for all types of underground constructions, but could also play a role in environmental investigations and have other purposes. Important information includes knowing the depth to the bedrock surface, its shape (even or irregular), whether or not it is fractured, lithological composition and degree of weathering. This type of information about the bedrock can be acquired by drilling, which is expensive, time consuming and provides information limited to the drill point. Areas between drill points must be extrapolated and may render inaccurate interpretations. With geophysical investigation methods such as geoelectrical methods it is possible to acquire a direct first-order overview of an area that could serve as a basis for further investigations.

The principle aim of this study is to investigate to what extent Direct Current resistivity and time-domain Induced Polarization (DCIP) can be used to characterize the bedrock at Önneslöv, which is located in Scania, southern Sweden. Additional methods, such as lithological borehole logs, borehole geophysics and magnetometry were used to strengthen and correlate DCIP results. The main bedrock features of interest are the depth to the bedrock surface, the occurrence of fractures and weathering zones and whether or not intrusive dykes can be observed from DCIP. The DCIP data will be inverted for spectral parameters with a Cole-Cole model using AarhusInv to investigate if the spectral inversion of IP data will give more information about the bedrock.

The data available has been acquired by the Engineering Geology department at Lund University in a project with Skanska because there is an interest in potential geoenergy storage in the study area. Knowing bedrock characteristics in advance is important because different materials and features in the ground can affect the construction and efficiency of the energy storage and could make planning more effective as well as reduce the construction costs.

2 Background

2.1 Regional Geology

The crystalline bedrock in southern Sweden (Fig. 1) was formed ca. 1.85-1.67 Ga ago and rocks in south western Sweden have subsequently been deformed and metamorphosed during events of orogenesis. The bedrock consists mostly of granitoid rocks and some mafic intrusions (e.g. Högdahl et al. 2004).

After the bedrock first formed in Sweden it has been reworked during both compressional and extensional events. The Hallandian orogeny was a compressional event which occurred around 1.45 Ga ago, in which Baltica presumably collided with an unknown continent in the south (e.g. Hubbard 1975; Cecys 2004; Brander & Söderlund 2009). After the Hallandian event another orogenic event occurred at 1.1-0.9 Ga, known as the Sveconorwegian orogeny (e.g. Johansson et al. 1991; Wahlgren et al. 1994; Möller et al.

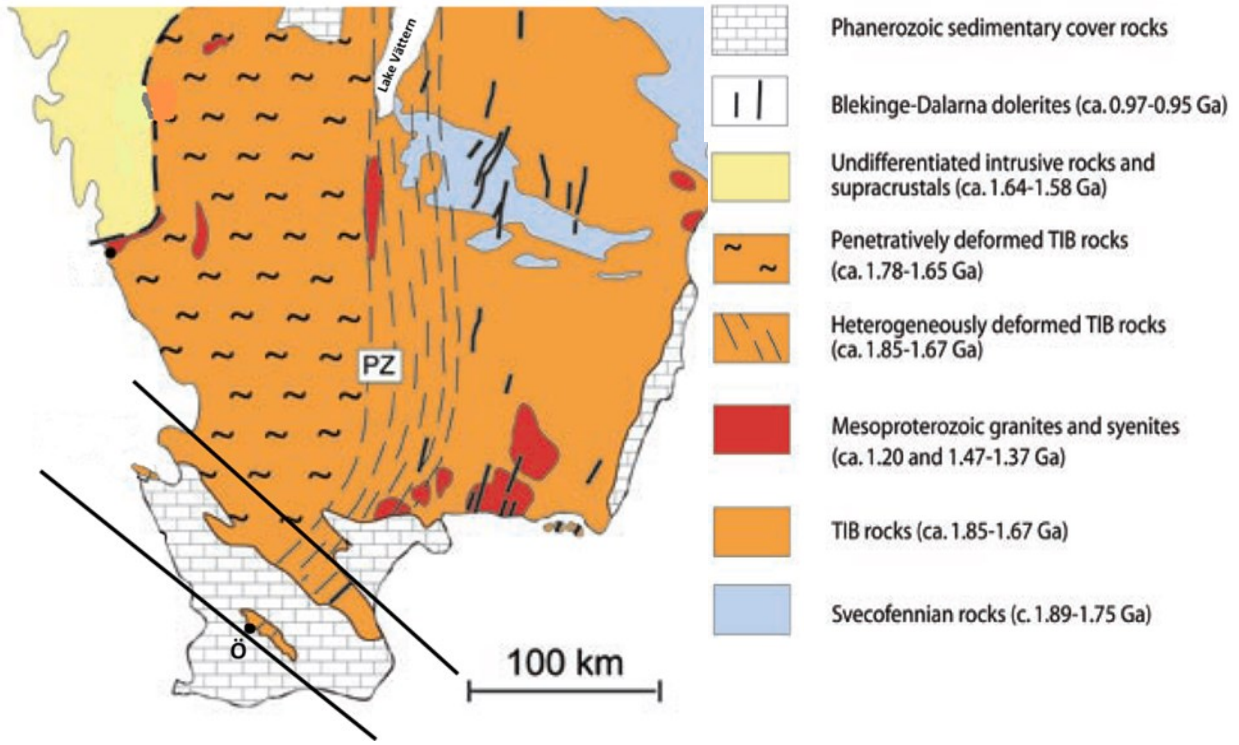

Figure 1. Simplified map of the geology in southern Sweden. Black lines are delineating the northern part of the Tornquist Zone in which the horst-graben system of Scania is exposed. The dashed lines depict the Protogine Zone (PZ). The point Ö shows the approximate location of the study area on the Romele horst. (Modified from Söderlund et al. 2008)

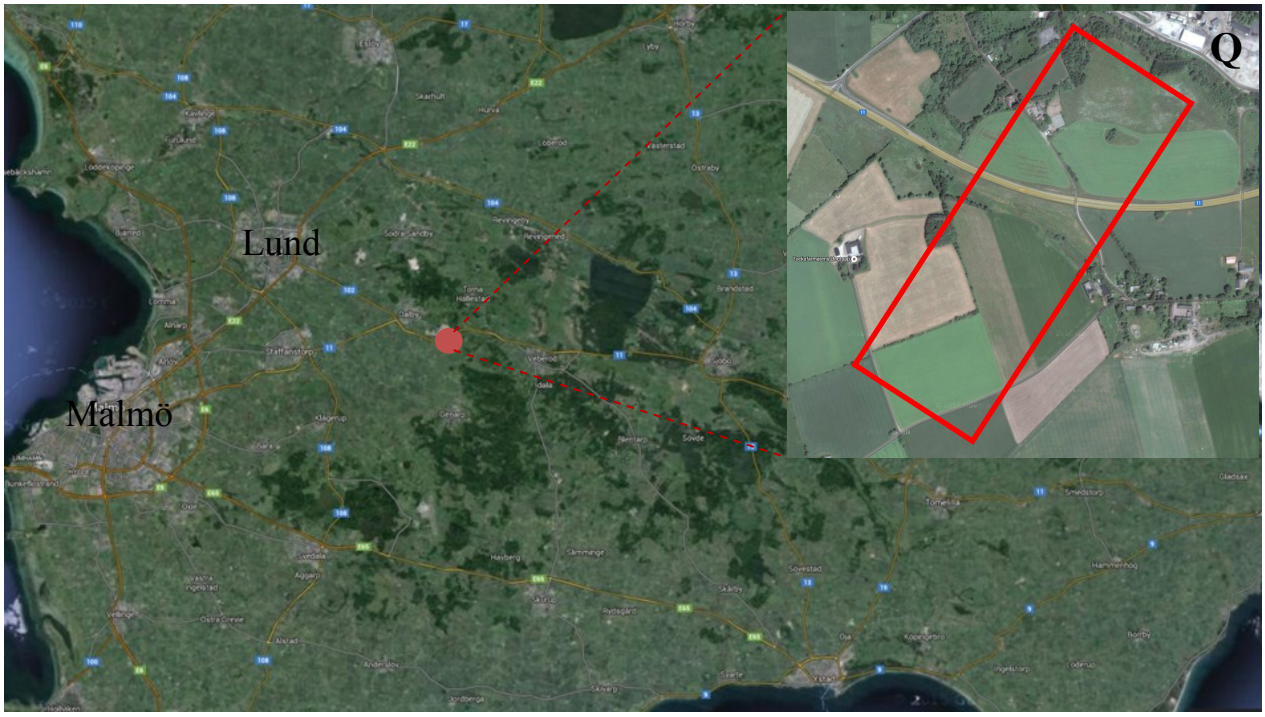

Figure 2. Map showing the location of the investigated area (red frame) in Scania in southern Sweden. The Q marks the Dalby quarry in the upper right corner.

2002). This is why south western Sweden is dominated by gneisses, which are metamorphosed rocks equivalent to pristine rocks of the Transscandinavian Igneous Belt (TIB) further to the east (e.g. Söderlund et al. 2002). The metamorphosed region is known as the Eastern segment and is part of the Sveconorwegian province.

The Protogine Zone (PZ) divides the bedrock of southern Sweden in the east and the metamorphosed equivalent in the west and has acted as a structural weakness zone for the most part of Proterozoicum (e.g. Gorbatschev 1980; Gaál & Gorbatschev 1987). South of Lake Vättern, the PZ is ca. 25-30 km wide and is defined by numerous shear and fault zones (Wahlgren et al. 1994). It also contain several pulses of intrusion that range in age between 1.56 Ga and 1.205 Ga (Söderlund & Ask 2006). The intrusions along the PZ have undergone various degrees of reworking and deformation due to the Sveconorwegian orogeny.

Another prominent structural zone in southern Sweden is the Tornquist Zone, which is made up of a system of NW-SE trending faults and shear zones that stretch from the North Sea, across Europe to the Black Sea. It has been active from ca. 300 Ma ago with alternating stages of compression and extension resulting in faulting and intrusion of mafic magmas (Bergerat et al. 2007). The faulting has also led to the formation of the horst-graben system that can be seen in Scania (Norling & Bergström 1986), with for example the Kullaberg- and the Romele horsts.

2.2 Study Area

The investigated area is situated just northwest of Önneslöv, a small community in the municipality of Lund, and ca. 1 km southwest of the Dalby quarry. The study area can be seen on the map below (Fig. 2).

2.3 Local Geology

The main rock type in the Dalby quarry is granitic gneiss. It is variably weathered from relatively fresh rock to clay. In Fig. 3a, one can see more intact but intruded and fractured gneiss to the left whereas to the far right the darker rock is strongly weathered. In the gneiss, several NE-trending mafic dykes can be seen. They are strongly deformed and amphibolitisised due to Sweconorwegian deformation (Fig. 3b). Locally, these dykes are very weathered and altered to clay. Attempts to date these reworked dykes using the U-Pb method on baddeleyite indicated an age of ca. 1.2 Ga (Cederberg 2011). Due to deformation, the dykes occur parallel to the regional deformation trend with the exception of dykes in bedrock lenses that escaped deformation (Fig. 3c). Post-Sveconorwegian diabase dykes are common in the quarry. These dykes have been dated at ca. 300 Ma (Klingspor 1976; Timmerman 2009; pers. comm. Söderlund 2016) and are trending in north western direction parallel to the horst-graben system in Scania. They are typically near-vertical and ca. 5-10m in thickness (Fig. 3d). The study area is located in the intersection between the Protogine zone and the Tornquist Zone and therefore most dykes in this location follow those two distinct directions (Fig. 1). Overlaying the bedrock in the quarry is a cover of till with a thickness of around 1-5 me-

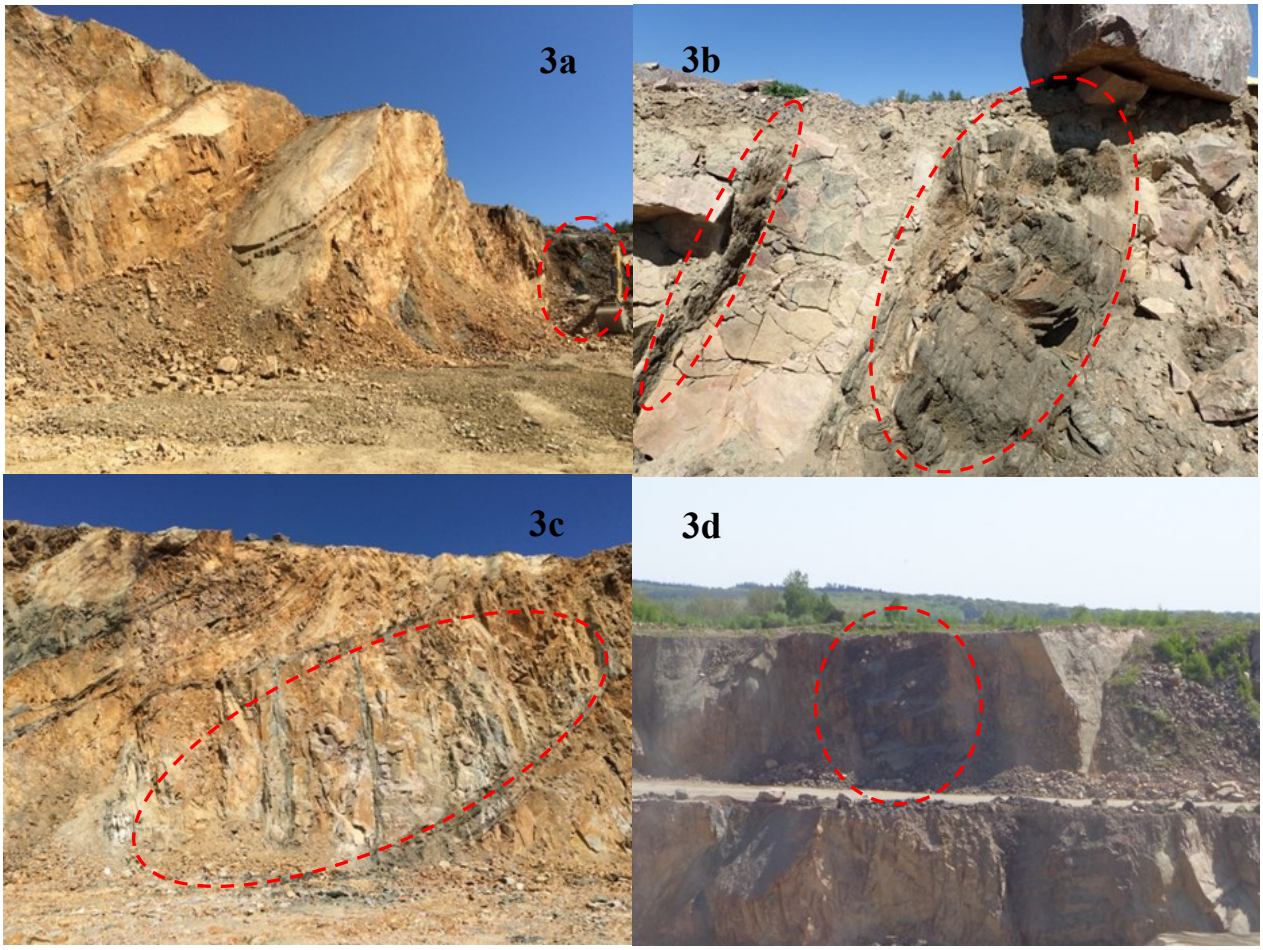

Figure 3. Photographs of the main lithologies in the Dalby quarry. 3a show relatively fresh gneiss, that is more clay weathered to the right (circled). 3b shows deformed and amphibolitisised dykes, where the right one is about 1m across. 3c shows a gneissic lens that escaped most of the deformation. 3d shows a NW trending diabase dyke about 10m across. (Photographs by Sara Johansson)

ters. The sedimentary cover is in general slightly thicker in Önneslöv. Because the studied area is situated very close to the quarry, it is assumed to have the same geological features as can be seen in the quarry.

Besides the main lithologies exposed in the quarry, there are several types of fracture mineralisations present. Halling (2015) identified 17 different minerals including carbonates, Fe-Pb-Zn minerals, epidote, chlorite, quartz, gypsum, and REE-minerals. She concluded that there have likely been several events of mineralisation related to contact metamorphism and hydrothermal activity.

3 Geophysics and Inversion Theory

Natural environments are made up of many different materials varying from solid rock to clay. The difference in material can also greatly affect the physical properties. Resistivity and induced polarization are two such properties. The resistivity survey method was developed in the early 20th century but was not widely used until the 1970s. It measures a materials resistance to conducting electricity (Reynolds 2011). The increase in usage in the 70s was due to increased computing power and improved methods. The resistivity method is used for various investigations such as search for groundwater, cavity mapping and archaeology. It is also used for environmental purposes, for example to investigate contamination situations at contaminated sites (Åkesson 2015).

Induced polarization measures a materials' ability to act as a capacitor. When a current is applied the material becomes polarized. When the current stops the charge of the material will go back to its initial state after a certain time (Reynolds 2011). In so called time-domain IP, this decay time is measured. In frequency-domain IP, the shape of the relaxation curve also gives additional information. The induced polarization phenomenon was discovered in 1913 by Conrad Schlumberger and has been used since the 1950s primarily for mining and petroleum exploration purposes (Reynolds 2011). Both due to improved measuring techniques and increased computing power, it has become viable in the last few decades to use in other types of investigations as well, such as environmental investigations and characterization of soil (Sharma 1997) and bedrock (Magnusson et al. 2010).

3.1 Resistivity

The resistance to electrical current in a material is a material dependent property and is called resistivity, with the unit ρ, measured in Ωm. If a material is completely homogenous, the measured value will be the *true resistivity*, however the occurrence of completely homogenous materials in nature is very unusual. True resistivity can be explained as the quota of electric field strength and current density (Eq. 1; Reynolds 2011). However, since most natural materials are heterogeneous and resistivity is measured over a volume, the measured value will be a mean value of all materials within the measured volume. The resulting measurement is called *apparent resistivity* (Reynolds 2011). Apparent resistivity can be defined as the product of the resistance R and a geometrical factor K (Eq. 2; Reynolds 2011). The geometrical factor depends on

Eq. 1 $\rho = E / J$ **Eq. 2** $\rho = R \cdot K$

the electrode configuration and therefore on the measured length and cross section, which means that the measurements are of a volume and not a point as is illustrated in Figure 4. Theoretically, the median investigation depth is defined as the depth which is reached by 50% of the current. The apparent resistivity is presented as a pseudosection, with a pseudodepth calculated from the electrode positioning and set up. To get an interpretable model from the pseudosection, inverse numerical modelling is necessary (see "3.3 Inversion modelling").

Since measurements are conducted along a line when using electrical resistivity tomography, structures in the ground have to be assumed to be in two dimensions, when in reality they are 3-dimensional. It

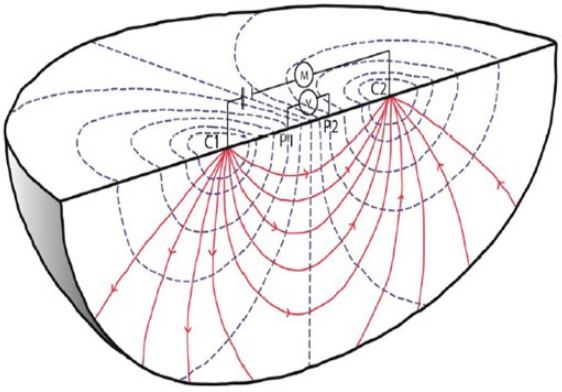

Figure 4. Figure illustrating the equipotential lines (dashed) and current paths (red lines) through the ground during resistivity measurement (Åkesson 2015).

is therefore important to lay the survey lines perpendicular to vertical elements in the ground and topographical highs and lows if possible. The geometry of the subsurface and the topography of the surface may otherwise give false measurements due to bodies of high or low resistivity and create so called 3D-effects (Sharma 1997). When interpreting resistivity data another difficulty may be that different geological materials can have the same resistivity values, or at least overlap to some extent as can be seen in Figure 5.

3.2 Induced Polarization

Induced polarization (IP) occurs when a material that has the ability to polarise is exposed to an electric current. The material will then charge up as a capacitor. There are two ways for this charge to occur. Grain polarization (Fig. 6a) is a surface process that occurs when there are conductive minerals present, for example metal sulphides. The grains will be polarised when

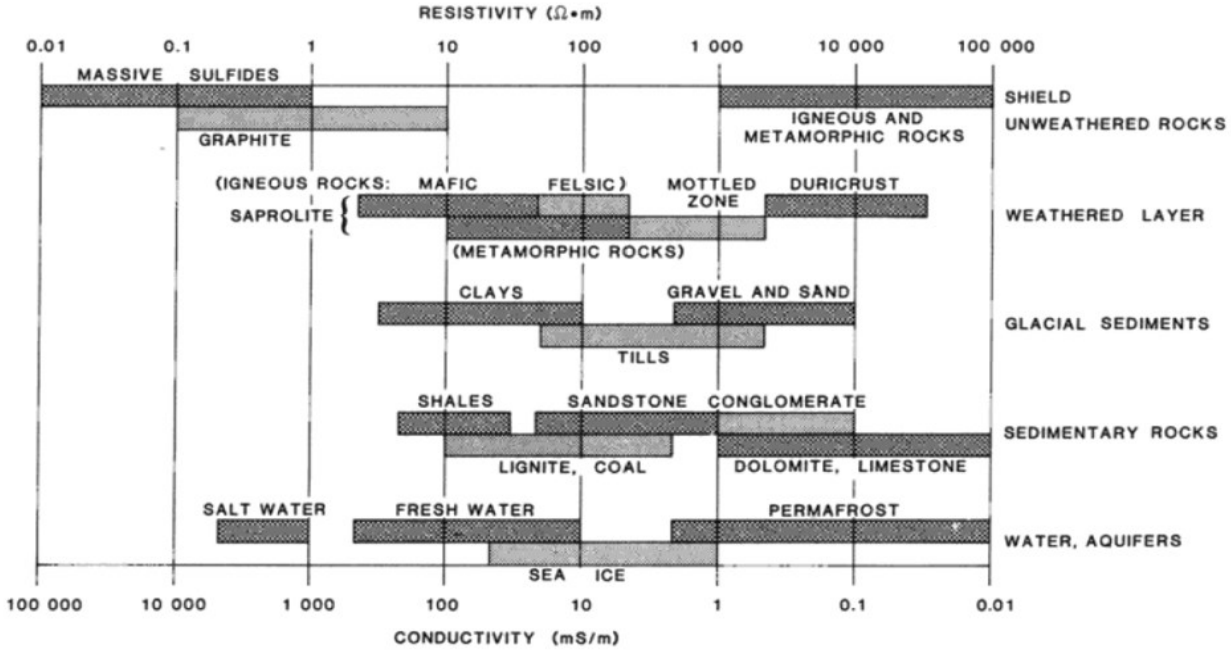

Figure 5. Generalised resistivity scales for different natural materials. (Palacky 1987)

a current is applied which in turn will attract opposing charges. Membrane polarization (Fig. 6b) is a process taking place between grains where the mass around the pore space becomes polarised making opposing charges block pore throats and in this way creating capacitors. Membrane polarization can also occur due to clay particles or other fibrous elements as the particles create a sphere of charges around them (Reynolds 2011). Since these processes are superimposed on each other, what is measured is the sum of all polarization processes (Johansson 2016). IP measurements are, just as resistivity, measured as *apparent IP* response because it is a measurement of a volume, most likely containing a number of different materials. The measurements are, as resistivity, presented as a pseudosection. It must therefore also be modelled using inversion modelling software to yield interpretable results (See "3.3 Inversion modelling").

There are two ways of measuring induced polarization, Time-domain IP and frequency domain IP. Time-domain IP is measured as the time it takes for the polarization effect to return to its initial state after the current is turned off (Reynolds 2011). It is measured as chargeability m with the unit mV/V, millivolts per volt injected. When measuring in time-domain, the decay curve is divided into gates or time windows, where a mean value is calculated for each gate.

Frequency-domain IP can also be called complex resistivity and measures the amplitude- and phase shifts between injected current and measured potential while applying an alternating current (Johansson 2016). This will not be discussed more as it is not within the scope of this thesis.

It has become possible to use models to describe frequency domain with the spectral parameters frequency factor *c* and time constant *τ (tau)*, in time-domain. The decay curve can be fitted to a so called Cole-Cole model, which is a generalised model that fits complex resistivity, but that also has been remodelled to fit time-domain IP (Eq. 3) (Pelton et al. 1978).

In this equation $V(t)$ stands for the voltage drop after the current (I_0) is shut off. m_0 is the intrinsic chargeability at the time the current is cut, and R_0 is the DC resistivity. C and τ help describe the shape of the decay curve, where C is the frequency factor and τ is the time-constant.

Eq. 3 $$V(t) = m_0 \frac{R_0}{I_0} \sum_{n=0}^{\infty} \frac{(-1)^n \left(\frac{t}{\tau}\right)^{nc}}{\Gamma(nc+1)}$$

τ (measured in seconds) describes how quickly the polarization decays after applied current is shut off and a low τ give a steep decay curve (Pelton 1978). C describes the shape of the decay curve and is a measurement of how homogenous the material is, because C depends on the frequency peak of a certain material. A homogenous material will therefore have a high C, as there is one main relaxation process, and in turn one main polarization process. Pelton (1978) found that the type of mineral does not affect the C very much and that increased grain size increases τ. Johansson et al. (2016) observed that spectral parameters could be connected to textural differences in limestone.

The IP response in a material is dependent on the material itself, but also on that the current is running through it. Since the current will take the path of least resistance, a more resistive material might show a lower IP response than it otherwise would. This can happen for example if fractures or sediments are filled with water, leading to the IP measurement looking lower than it should be if the material was dry. To resolve this issue, Slater & Lesmes (2002) proposed to use *Normalised IP*. Normalised IP is the IP effect divided by the resistivity and will show the IP effect of the material itself without the "quicker electrical paths", accentuating the polarization effect of the material. Essentially, it shows the surface polarization of the material measured in mS/m.

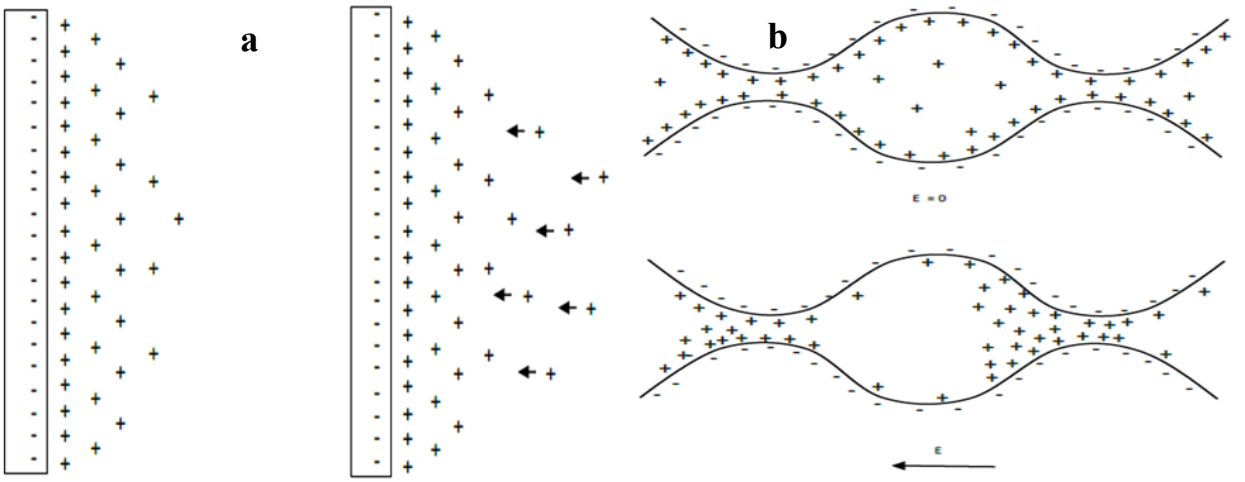

Figure 6. a) Grain or electrode polarization, where an applied current will attract opposite charges to the surface of a material. Modified from Johansson (2016). b) Membrane polarization. Upper: no current applied. Lower: applied current makes opposite charges attract and block pore throats. (Johansson 2016)

Recent developments in measuring techniques and signal processing have made it possible to improve IP data significantly, making spectral analysis more viable. Furthermore, separating current and potential cables can improve data quality by lowering capacitive coupling effects (Dahlin & Leroux 2012). The improvements in processing include removal of non-linear drift, harmonic noise, and spikes (Olsson et al. 2016). Processing also makes it possible to use earlier and later times of the decay curve, giving more information than previously was possible. It has also been concluded that measuring the IP during current injection using a 100% duty cycle instead of 50% duty cycle can be used for spectral analysis but also improves data quality (Olsson et al. 2015).

3.3 Inversion Modelling Theory

In order to receive interpretable results from pseudosections, inversion modelling is necessary. Before the inversion process, data processing is usually needed since erroneous data points may be present. Also topography data should be added to correct for irregular topography that could influence the data (Reynolds 2011).

During inversion, a starting model is assumed with a number of layers, divided into blocks, in the ground based on the pseudosection and pseudodepth. The size of the layers and blocks depends on the electrode spacing and number of data points, and is increasing with depth. AarhusInv then uses finite element modelling (Fiandaca et al. 2012), which creates a pseudosection based on the assumed model and compares it with the measured data pseudosection. It could be explained as that the program uses information of how measurements were taken, and the data aquired from measuring, and tries to find a realistic distribution in the ground that fit the data. How the realistic distribution will look also depends on what constraints are set before inversion. This process is repeated, with a number of iterations altering the model until the model fits the measured data as well as possible, or until the misfit is below pre-set acceptable values. The misfit is presented as percentage RMS (root-mean-squared) error between the measured data and the model (Reynolds 2011).

It is important to keep in mind that the Cole-Cole model in AarhusInv (Fiandaca et al. 2012) uses the unit m_0 and not m for IP, which means that instead of calculating an integral chargeability over a chosen time frame, as is commercially common, the program calculates the polarization right after the current is cut. This will give IP values that are higher than in other kinds of software, for example Res2DInv (Loke et al. 2003, Geotomo Software 2015). This simply means that the values themselves should not be directly compared to results from different softwares. When integral chargeability is used, the pulse length also affects the magnitude of the results making comparison difficult (Olsson et al. 2015 B).

3.4 Uses of Resistivity and IP for Bedrock Interpretation

Resistivity and IP measurements have shown potential for interpreting bedrock features such as fracturing, presence of dyke intrusions, weathering zones and the bedrock surface. It was concluded in Magnusson et al. (2010) that there is a correlation between resistivity and amount of fractures giving lower resistivity with the presence of clay particles and/or water in fractures. Dry fractures would give a higher resistivity due to the lack of paths for the electricity to take. The same conclusion can be found by Magnusson et al. (2010) and Cegrell & Mårtensson (2008). It was also concluded by Cegrell & Mårtensson (2008) that mafic dykes can be detected by resistivity and IP, where mafic dykes would give high resistivity and low IP and that the proximal areas could have increased fracturing and mineralisations. In Rønning et al. (2013) a characterisation model is proposed for resistivity in crystalline bedrock where a resistivity of over 3000 Ωm is solid rock with low fracture frequency, 3000-500 Ωm is rock with more or less high fracture frequency with water in them and under 500 Ωm is fractured rock with water and clay weathering.

As proposed by Slater & Lesmes (2002) normalised IP could be of use in cases where quicker electrical paths minimize the polarization effect of materials. It can be helpful detecting clay content and weathering zones in a water saturated environment since clay has a large surface area but will, due to the water content, not show a distinct IP effect. It was also concluded by Bohlin & Landen (2008) that clay weathering can be found using normalised IP.

4 Method

4.1 Field Measurements

4.1.1 Magnetometry, Percussion Drilling and Borehole Geophysics

Magnetometry has previously been performed by Sweco at the Önneslöv site and the interpretations from this study will be used as an additional help for interpreting the resistivity and IP results. Additionally, seven percussion drillings, between 130 m and 250 m depth, were performed by HP Borrningar AB for Sweco. The lithological records from these drillings are used for an overview of the bedrock in the area and to help strengthen interpretations of fracture and weathering zones.

Geophysical borehole logging has been performed by the Engineering Geology department at Lund University in three of the boreholes, HB02, HB03 and HB05. The natural gamma and especially caliper logs are used as additional data to strengthen the interpretation of the other methods, especially for weathering and fracturing. The natural gamma log is for example usually used for detecting clay content in sedimentary formations and to measure purity of sand

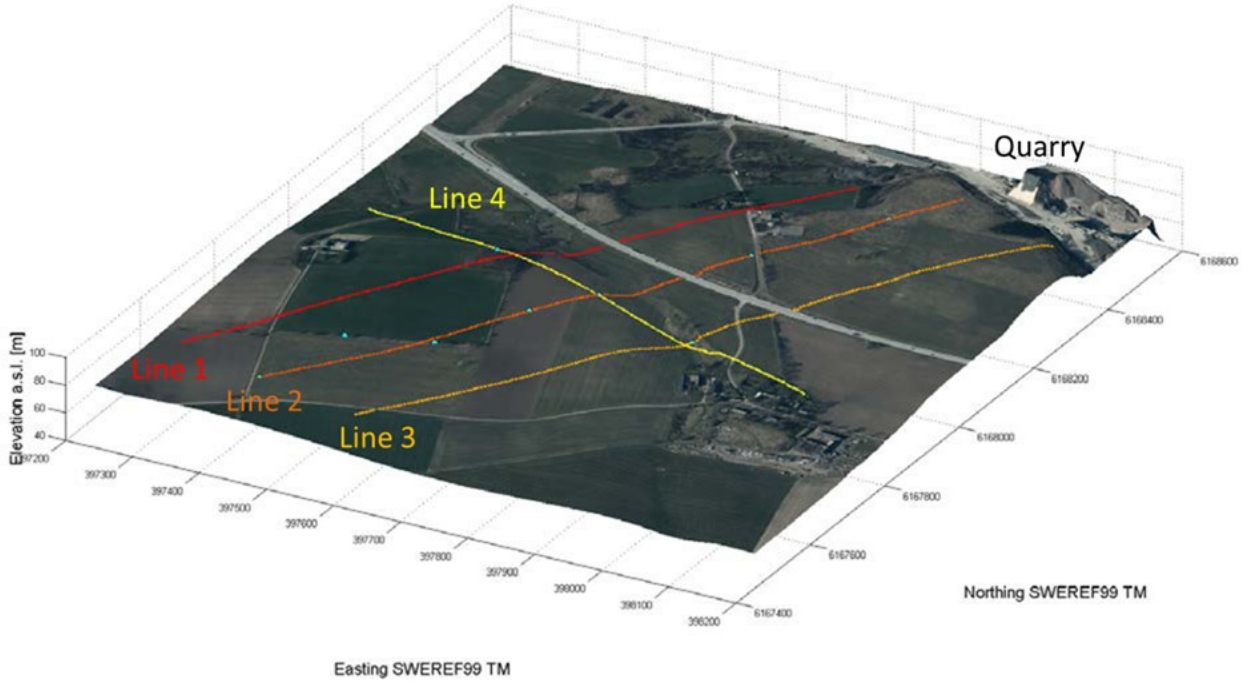

Figure 7. Map with topography over the investigated area at Önneslöv. Survey lines and location of Dalby quarry are marked. (Image by Matteo Rossi, Engineering Geology, Lund)

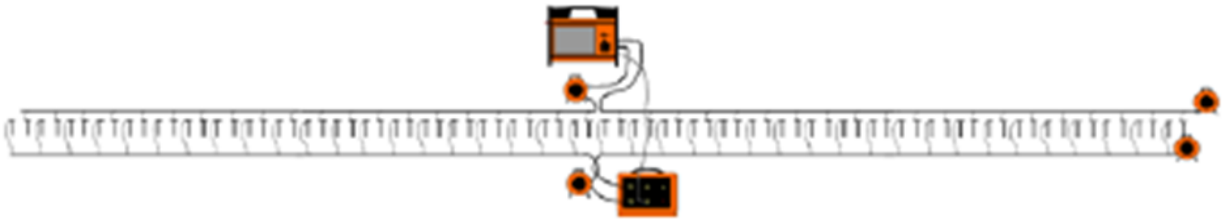

Figure 8. Schematic image of multi-electrode measurement, using separated cables (Johansson 2016).

formations (Reynolds 2011). However, since sedimentary rocks are not present in the study area it could give a better idea of the minerology instead. The caliper log is a mechanical log that measures the width of the borehole and will show cave-ins due to fractures and weathering and thereby give information on the stability of the ground (Alm 2012).

4.1.2 Resistivity and IP Measurements

In Önneslöv, resistivity/IP line surveys were conducted by members of the Engineering Geology department at the Faculty of Engineering at Lund University. In this master thesis the data from these survey lines are used. Three layouts were conducted in the northeast-southwest direction and one in the northwest-southeast direction. The layouts intersect. The three survey lines in the northeast-southwest were 1000 meters long and the northwest-southeast line was 800 meters long. The electrode spacing was 5 meter. The layouts of the survey lines can be seen on the map in Fig. 7.

The instrument used was an ABEM TerrameterLS. Stainless steel electrodes were used. Separated multi-electrode cables were used for current and potential when measuring in order to reduce capacitive coupling effects (Fig 8). The measurements were conducted with a multi-gradient array protocol where both current and potential electrodes are moved to measure different positions and depths (Dahlin & Zhou 2006). The pulse length was 4 seconds with three cycles. Additionally, the measuring was conducted with a full waveform for current injection which improves data quality by amplifying IP effects and allowing for more stacks (Olsson et al. 2015 A).

4.2 Data Processing

The raw data acquired at the site was processed in two steps. The first step was made by the Engineering Geology Department where the data was put through a series of filters and signal processing. The aim of the processing was to correct for drift occurrences, to remove spikes caused by for example external electrical sources, and to remove the effect of harmonic noise and coupling effects. This was done in order to improve the data quality but also in order to extract the very early and late times of the decay curves that are otherwise unavailable for use (Olsson et al. 2016).

The second step in the processing was to remove decay curves or parts of decay curves that are

considered to be of low quality or false. So called outliers, for example, are IP decay curves that do not match the other curves at all and are therefore considered to be false measurements. This processing was done via the program Aarhus Workbench (Fiandaca et al. 2012). Due to unreliable data in the very early acquisition times, the first 5 gates, around 5 ms, were removed before further processing. Some decay curves were removed completely according to certain criteria. These criteria were if the curve changed sign, did not have an exponential decay, or fit badly with other curves. In some curves only individual gates were removed. In these cases, a portion of the curve, usually the beginning or end, was not to be trusted if it unexpectedly differed strongly from the general curve shape. Also, at 80 milliseconds a systematic dip in the IP measurement occurred that could not be explained within the aim of this thesis therefore all values at 80 milliseconds were removed. In most cases a dip that could not be explained was also observed in the very last gate and therefore this last gate was also removed. In the inversion, all negative decay curves were removed after seeing that they rarely fit in preliminary attempts.

During manual processing, data were removed before final inversion. In total, 43% of data from survey line 1, 30% from line 2, 22% from line 3 and 37% from line 4 were removed. The reason for the high amount of removed data is, partially because all data in two gates were removed which equal around 10%, but also because a conservative approach was taken to ensure that the data that is left is to be considered of high quality. Some of the decay curves and time windows removed might have contained good data, however it is still not fully known how the different polarization processes work and therefore not fully known which data can be trusted.

4.3 Inversion Modelling

After the data was processed, it was inverted in AarhusInv (Fiandaca et al 2012) via Matlab as 2D inversions with a Cole-Cole model. The model parameter used was “L1 Loose”, which is a finite element model using somewhat looser constraints. In order to accentuate differences in the model even more, both the vertical and horizontal constraints were set looser than in the original settings. Usually, the program smoothens out sharp differences. However, since sharp vertical structures are believed to be present here the settings were changed.

5 Results and Interpretation

5.1. Magnetometry Results

In the studied area, magnetometry was performed and interpreted by Sweco. The interpretations indicate that there are several dykes going in a NW-SE direction. Five of which have given major anomalies and four with lesser anomalies. Examples of major and minor magnetic anomalies from survey line 3 can be seen in Fig. 9. The ones giving a major signal has been interpreted by Sweco as NW dykes, and the ones with minor signals as minor anomalies that can be connected at least in the centre of the profiles. Therefore, minor anomalies could be dykes but this is not certain. Some magnetic anomalies are present in the profiles that are not connected as linear elements in the interpretation. Therefore all anomalies are marked in the profiles below. No NE-SW dykes have been interpreted. The major anomalies are mostly situated in the beginning of or in the second half of the profiles one, two and three. The minor anomalies are mostly situated in the centre of these profiles, with the exception of profile one where several also are towards the right end of the profile.

The positions of the interpreted dykes (major anomalies) and minor anomalies are shown in the inverted profiles below, in "5.4. Inversion results", with purple and yellow marks in the profiles. Purple indicates a strong anomaly (dyke) and yellow a minor anomaly.

5.2 Borehole logs

The lithological percussion drill logs are listed in Table 1 and presented in the inverted profiles below in "5.4. Inversion results" where they are marked approximately. Due to resolution issues the soil depth is presented in Table 1 and the borehole lithology is simplified in the profiles. For a more detailed description see Appendix B. Boreholes that are located in intersections between profiles are marked on both profiles. According to the borehole logs the soil depth in the area is between 4.6m and 25m. However, six of the seven boreholes have a soil depth of less than 10m. Furthermore, parts of the bedrock are weathered to various states and fractures are numerous. There are numerous amphibolites of different thickness present

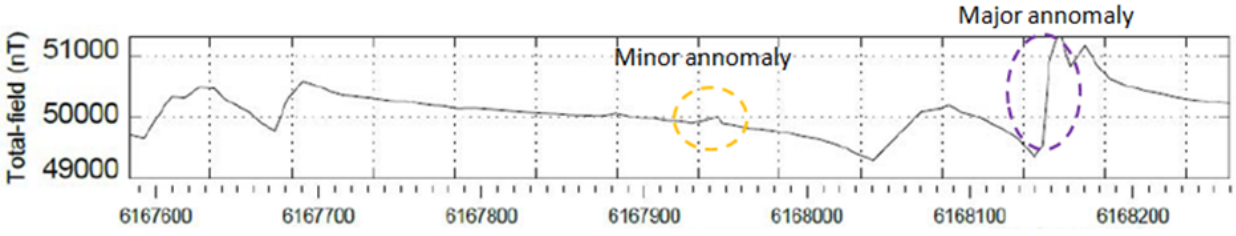

Figure 9. Magnetometry data over part of profile 3. Circles show examples of anomalies where the yellow circle is the minor anomaly at 450m and the purple circle the major anomaly at 700m.

in most of the boreholes and they are located at various depths. Larger sections of amphibolite are marked separately but smaller ones are mixed in with the gneiss as "gneiss with amphibolites" and from what can be seen in the Dalby quarry the many amphibolites in the gneiss are most likely weathered and highly deformed. One borehole, HB06, is omitted because it has an offset of 200m westwards from profile 2, however it is included in Appendix B.

Table 1. Summary of percussion drill logs' positions along the survey lines and the soil depth for each location.

Name	Position	Soil depth	Borehole depth
HB04	Profile 2, 240 m	5.5 m	220 m
HB02	Profile 2, 485 m Profile 4, 420 m	6.7 m	246 m
HB05	Profile 2, 700 m	25 m	250 m
HB07	Profile 2, 890 m	11 m	242 m
HB01	Profile 1, 480 m Profile 4, 240 m	9.5 m	172 m
HB03	Profile 4, 585 m Profile 3, 480 m	4.6 m	201 m

5.3 Borehole Geophysics

Since the bedrock in the area is crystalline and not sedimentary, the radiation levels seem to reflect the mineralogy and not the clay content of the formation. It is possible to distinguish two distinct different signatures connected to the rock type. The first has 70-125 CPS (counts per second), and correlates with mostly red gneiss from the lithological logs. The second has between 20-100 CPS and correlates well with grey gneiss. Other rock types, however in much smaller quantity, are present but difficult to distinguish since they fall into the same span as the gneisses. For example red gneiss rich in quartz gives a lower radiation count than gneiss without as much quartz. Grey gneiss with more muscovite gives a higher radiation than gneiss with less muscovite. Examples of the gamma signatures of the first 140 m from HB03 are presented in Fig. 10 below. The full gamma ray and caliper logs are presented in Appendix C.

The caliper logs show that the rock walls of the borehole often vary 1-3 cm in width. Only the most rigid parts of the boreholes lack or have less of this variation. HB02 has smaller consistent variations in diameter the first 80 m, apart from individual fracture zones at around 60-80 m depth. Further down, the borehole is less stable with larger fracture zones to a depth of 160 m. From 160 m to 240 m, the borehole is again stable with minor fractures. HB03 show variations in the caliper log with decreasing magnitude down to a depth of 105 m. Between 20m and 30m there is a larger fracture zone, and below that, around 70 m of varying degree of weathering making the borehole diameter vary 1-6 cm. Below this depth the walls are mostly stable apart from fracture zones at 120 m - 130 m, 160 m - 166 m and a fracture at 190 m. In HB05 the walls are unstable to a depth of 104 m varying in diameter 1-5 cm with a larger fracture zone at 92 m - 104 m. Below 104 m the variations are smaller, apart a fracture at 182 m.

The variations in diameter of a few centimetres in most cases correlate with weathering in the lithological logs or larger fracture zones, or a combination of the two. In general the lithological logs show that most of the upper halves of the boreholes are weathered to some extent. An example of the caliper and gamma logs from HB03 can be seen together in Fig. 10 below.

5.4 Inversion Results

The inverted profiles 1-4 are presented individually below, after which they are presented in a combined manner in order to show how the structures in the ground fit together. The magnetrometry results have also been added to the inverted profiles as the purple and yellow points along the profiles, where purple indicates a strong magnetic anomaly and yellow a minor one. Percussion drillings that have been performed in the area are shown in the profiles as simplified logs. It is important to remember when looking at the inverted profiles that the precision is lower with increasing depth and towards the sides of the profiles. With increasing depth, the lack of data points causes cells to be larger, meaning that resolution decreases. In order to give an estimate of where the inversions are more trustworthy, two dashed lines have been added to the profile. The bottom one (grey) shows how deep the data points reach in the pseudosections. The upper one (orange) is an estimate of the depth at which a high density of data points can still be found. Since a pseudosection shows a theoretical depth depending on electrode configuration, the lines should be considered estimations.

The data misfit in the inversions was 8.3% RMS error in profile one, 15% in profile two, 25.1% in profile three and 7.4% in profile four. The misfit cross sections are presented in appendix A. In general, the resistivity has a better fit than the IP. The high misfit in the IP could depend on a few factors. First of all, not all unrealistic values were removed in the processing, creating some spikes. Secondly, it seems difficult for the inversion software to fit the very early acquisition times well. Another possibility is that the

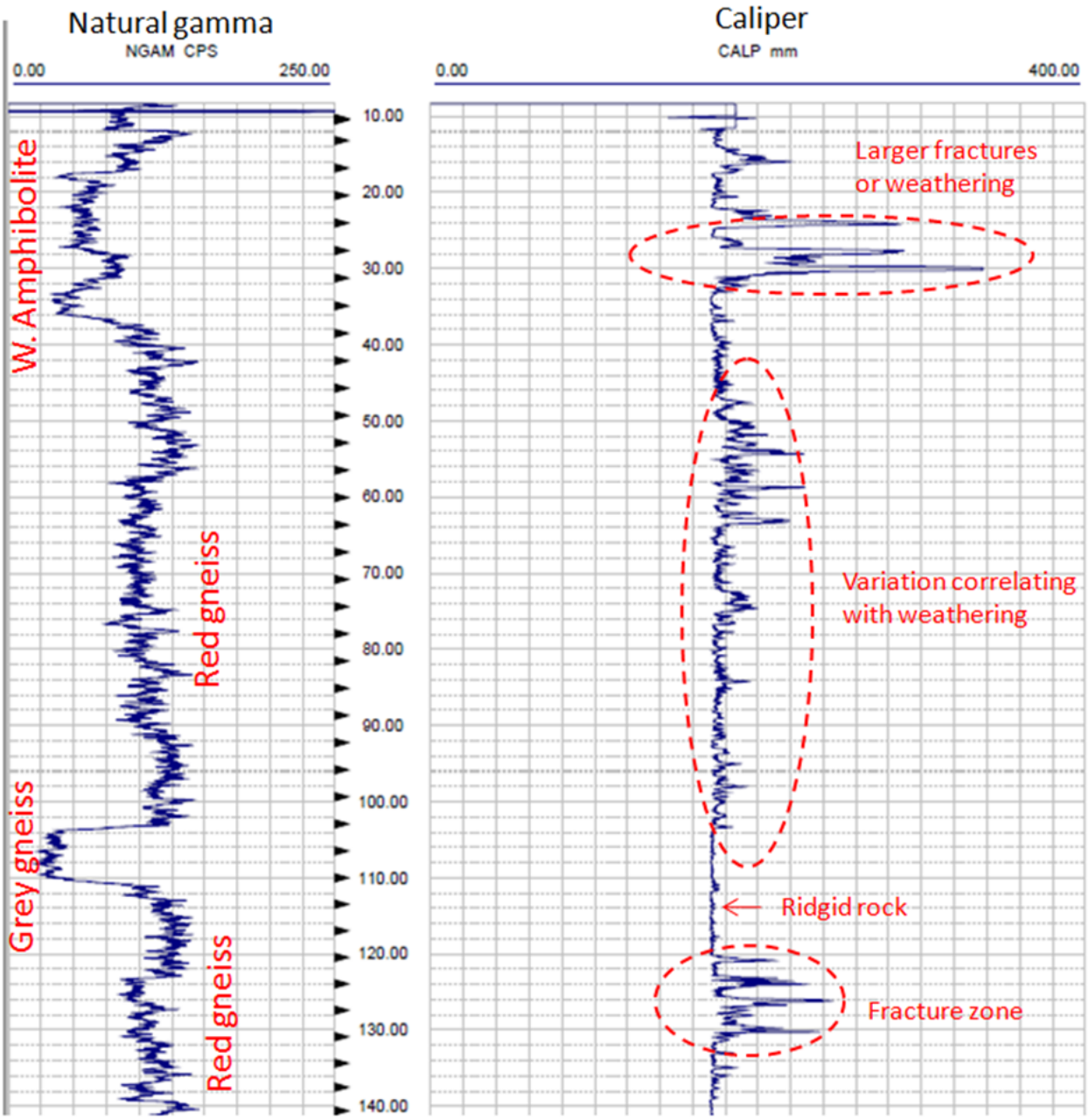

Figure 10. Example of gamma radiation signatures and caliper log from HB03. As can be seen there are 2-3 distinct gamma signatures correlating relatively well with lithological record for red gneiss and grey gneiss. The amphibolite often has similar levels to grey gneiss, but varies more. The caliper show that most of the borehole has some form of weathering and 2-3 sections with larger fractures or cave-ins. W = Weathered.

data values are varying strongly and that the constraints in the inversion make it difficult to fit well.

5.4.1 Profile 1

Profile one (Fig. 11) shows a generally highly resistive ground with areas of lower resistivity that can be seen at around 220 m and 700 m. In the central part just by the borehole, a small, low resistivity zone can be seen at very shallow depth. In the centre there is also an area of lower resistivity at around 100 m depth where the ground is otherwise of higher resistivity. The IP response looks similar to the resistivity with zones of higher IP values in the edges of the profile and a distinct high zone in the middle. As well as for the resistivity, the zones of higher IP are divided by areas of lower IP at 220 m and 700 m. The upper part of the profile has generally low resistivity and varying IP. In the borehole, HB01, the upper 50 m of the bedrock contain gneiss with amphibolites and a larger amphibolite section containing epidote as fracture mineralisation. Below this level, the main rock type is unweathered gneiss.

For the most part, τ gives lower responses when resistivity and IP also are lower. However, this is not very clear. The upper part of the profile shows low τ values, ranging to the lower end of the scale along most of the profile. Generally C is lower when the IP

is lower, for example at x=700 m. The normalised IP (lowest profile in the Figure), shows a zone of higher normalised IP in the centre at x=500 m in the same place as the IP also was high. At x=700 m the normalised IP also shows elevated values correlating with the resistivity and IP low zone. In between these two areas there are elevated values mainly in the deeper parts.

5.4.2 Profile 2

Profile two (Fig. 12) also shows a ground of higher resistivity divided by zones of lower resistivity at x=200 m and x=700 m. Other more shallow anomalies of lower resistivity can be seen at, for example x=100 m and x=450 m. The IP response show three features along the profile. At around x=250 m, there is a diffuse area of lower IP. Between x=400 and x=600, the IP is increased, especially in the upper left parts of which some correlate with one of the shallow resistivity anomalies. A slight increase in the IP can also be seen as a vertical element at around x=820 m. Generally, the very upper parts of the profile show low resistivity and lower IP, however the IP has less contrast to underlying layers compared to the resistivity. In some areas such as the resistivity low zones, the transition to higher resistivity is also very diffuse.

HB04, to the left in the profile, show gneissic unweathered bedrock apart from between 34m and 70m depth, where the gneiss also contains some amphibolites. In HB02, similar gneissic bedrock can be seen, however the upper part, between 7 m and 28 m, is weathered. In HB05, which is situated in the large zone of low resistivity, the bedrock is weathered until 107 m below the surface. Below the weathering zone mineralisations can be found in fractures until 124 m, after which fresh gneiss continues. HB07, the rightmost borehole is weathered in the uppermost part until 23 m, after which the bedrock is mostly gneissic, but containing several minor amphibolite dykes.

τ shows few changes apart from some areas in the upper layer, such as at x=450 m where the lower τ somewhat correlate with low resistivity and a minor magnetic anomaly. It is also slightly lower around the larger areas of lower IP. C follows the same pattern as in profile one with a lower signature in the areas of lower IP. In the shallow parts, C is in some cases also lower where IP is lower and a minor magnetic anomaly can be found, for example at x=450 m and x=500 m. The normalised IP shows four shallow zones of elevated normalised IP that stretch around 30-50 m down, at x=100 m, 200 m, 450 m, and 700 m. They correspond to the same areas of low resistivity and the first three also fit magnetic anomalies well. At x=750 m there is, however, a slightly deeper normalised IP anomaly that fits a, by magnetometry, interpreted dyke well.

5.4.3 Profile 3

In general profile 3 (Fig. 13) also has ground with high resistivity. The leftmost area of the profile also has higher resistivity but not as clear as in profiles one and two. However, it can be seen until around x=150 m. There are two areas of lower resistivity dividing the highly resistive ground, one more shallow around x=200 m that looks to be two low zones which blend together, and one areas that stretches deeper at around x=750 m. Apart from these large areas, there are again more shallow areas at x=60 m, x=420 m and x=480 m with lower resistivity, which coincides with magnetic dyke interpretations or minor magnetic anomalies. The IP response in profile three shows slightly less variation than in profile one and two. However, similar elements can be seen. Lower IP can be found in the area around x=200 m, where resistivity is also. Higher IP is present especially in the centre of the profile and coincide at x=380 m with higher resistivity and at x=420 m with lower resistivity and a minor magnetic anomaly. There is also a vertical area of higher IP at x=720 m, close to a dyke, similar to what can be seen in profile two. The borehole, HB03, shows gneissic bedrock with an amphibolite zone at 21 m to 39 m and some smaller amphibolites after that. In the caliper log, this larger amphibolite zone either has a larger fracture zone or is very weathered since the borehole diameter increases up to 17 cm. The bedrock is also weathered down to 110 m. However, the degree of weathering decreases with depth which can also be seen in the caliper log. At 120 m-130 m of depth there is a fracture zone, but otherwise the borehole is relatively stable below 105 m apart from some fractures.

τ changes very little along the profile but shows two zones of somewhat lower signal. The first is the diffuse area around x=200 m - 400 m, similar to the area of low resistivity and IP and the second is at the vertical higher IP area at x=720 m. C is lower in the area of low resistivity and IP at around 200 m - 300 m and other smaller low areas in the very shallow layer can also be seen.

The normalised IP in profile 3 also has a few shallow areas with elevated normalised IP that correspond with low resistivity zones and reach approximately around 40 m down, in most cases also coinciding with magnetic anomalies. The larger area of elevated normalised IP at 600 m – 700 m on the right side of the profile corresponds well with the low zone in the resistivity and is similar to the same area in profiles one and two.

5.4.4 Profile 4

Profile four (Fig. 14), the perpendicular profile, shows a shallow zone of lower resistivity that relatively sharply changes to higher resistivity below. Deeper, below 50 m – 80 m, for most part of the profile, resistivity is intermediate. Between x=480 and x=640, however, there is an area of high resistivity below this level. To the right of this area to the end of the profile the resistivity is low. The IP has a top layer of low IP that correlates with the low resistivity. There are two larger areas of higher IP at x=80 m – 160 m, and at x=240 m – 400 m that coincide with somewhat lower

resistivity values. In the right zone of high resistivity at x=480 m – 640 m the IP is lower in the more shallow parts. The rightmost part, from 640 m shows lower IP however with a slight IP high zone that correlates with a small increase in resistivity around 50m down.

The boreholes along profile four are HB01, HB02 and HB03 since they are situated in the intersections of the profiles. For the most part the bedrock is gneissic with the exception of amphibolites in the upper parts of HB01 and HB03. Minor amphibolites also occur deeper. Depending on the area in between HB02 and HB03, the depth of weathering looks to be increasing towards the right in the profile. The Caliper logs, however, show larger variations in HB02 down to 160 m compared to HB03. The shallowest layer in the boreholes, most likely the soil, also correlates well with the top layer of low resistivity.

τ gives a lower signature, where the IP is lower. That can be seen in the upper ca 30 m - 40 m and is especially low in the very top layer, similar to profile one. C shows high values for the most part, except for the upper layer, similar to the τ, and correlate well with the lower IP areas. The normalised IP shows three distinct elevated areas. Two of them correlate well with the drawn out high IP areas in the left half of the profile and the third coincides with areas of low resistivity and IP to the right.

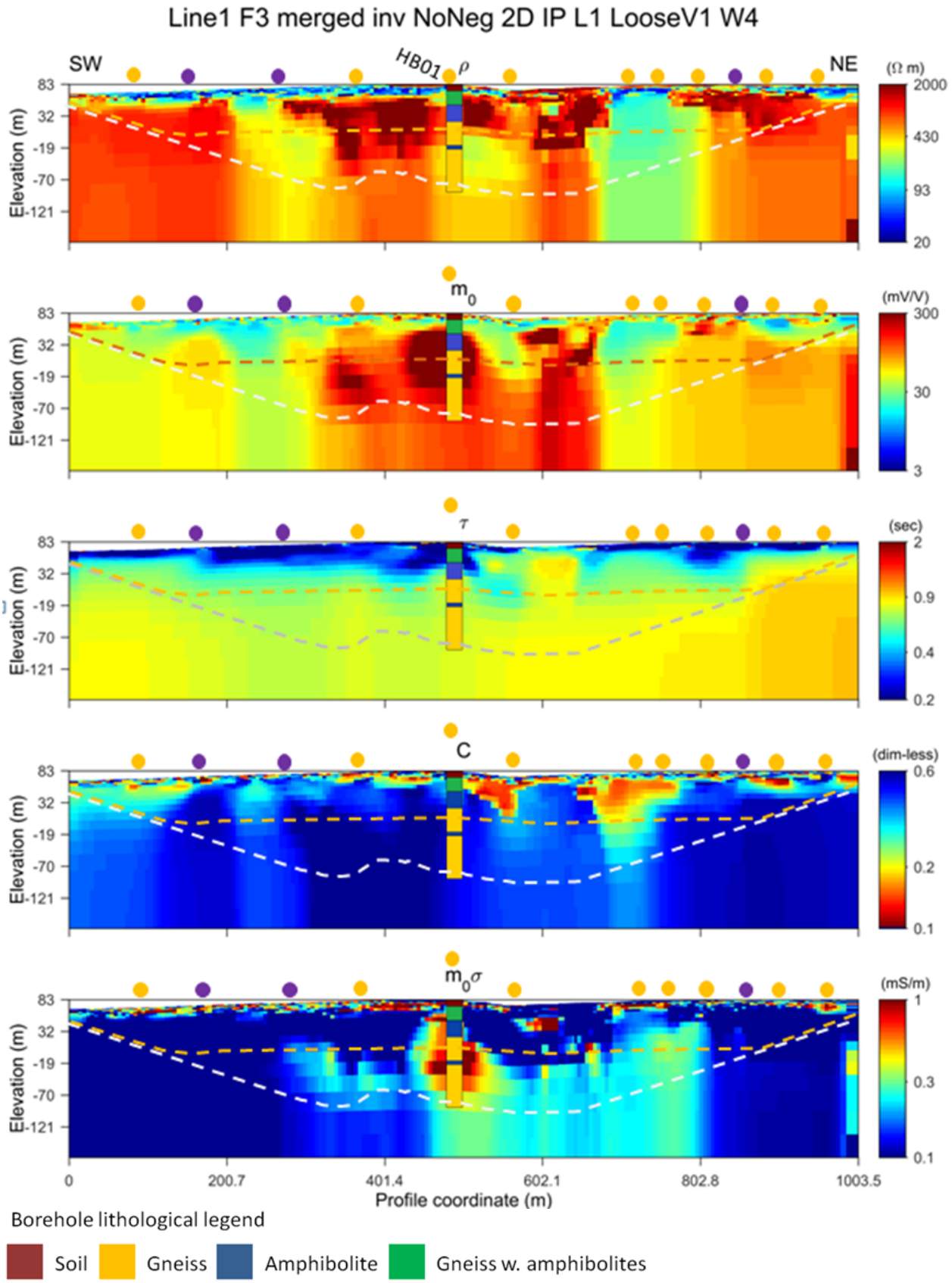

Figure 11. Inverted 2D profile for survey line 1 showing from top to bottom resistivity, IP response, τ, C and normalised IP. Purple and yellow points are magnetic results showing strong or weak anomalies. Borehole HB01 is marked with simplified lithology. The grey dashed line shows the deepest data points and the orange dashed line shows the threshold at which density of data points is still high.

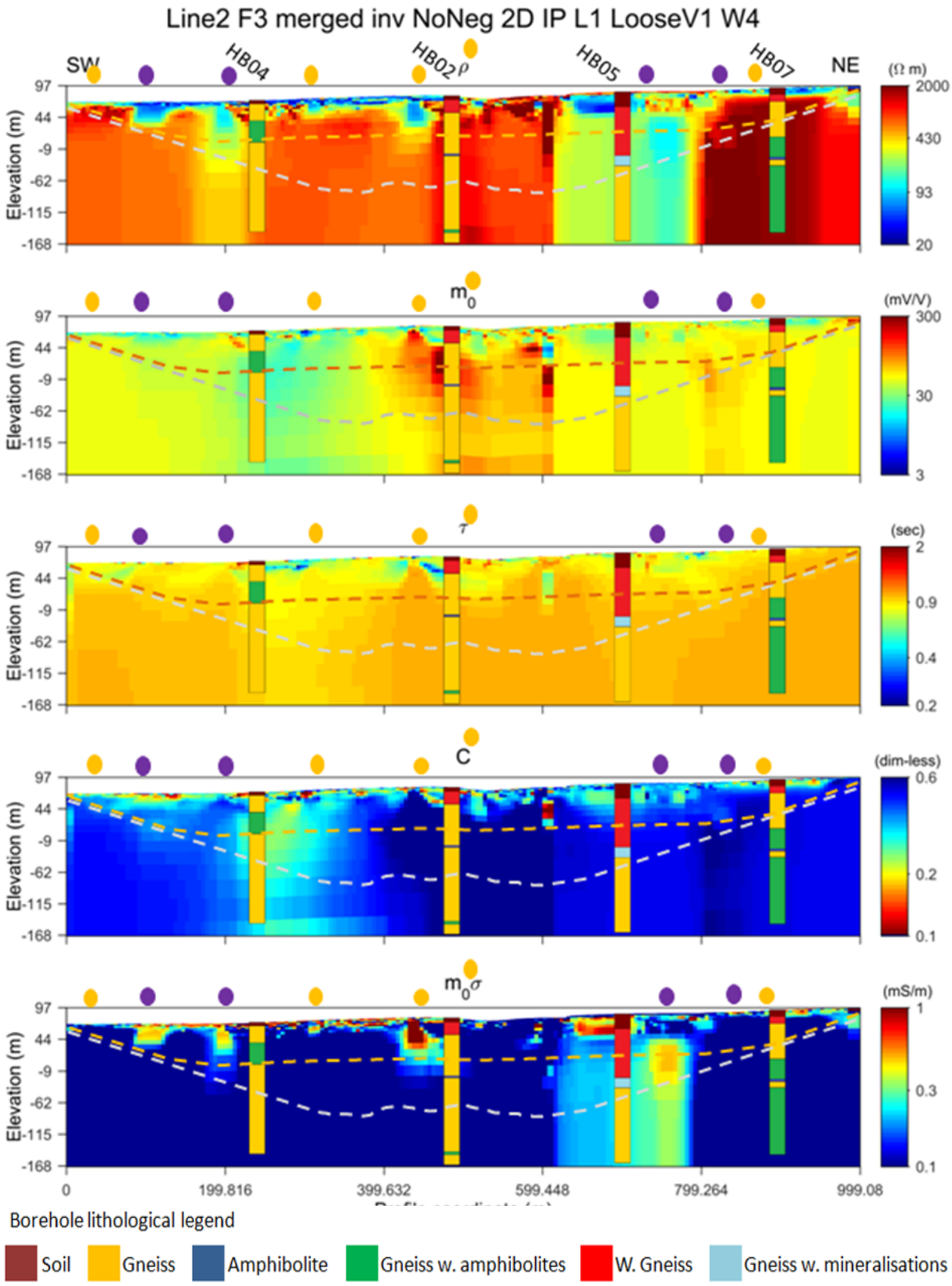

Figure 12. Inverted 2D profile for survey line 2, showing from top to bottom resistivity, IP response, τ, C and normalised IP. Purple and yellow points are magnetic results showing strong or weak anomalies. Boreholes HB04, HB02, HB05 and HB07 are shown with simplified lithology. The grey dashed line shows the deepest data points and the orange dashed line shows the threshold at which the density of data points is still high.

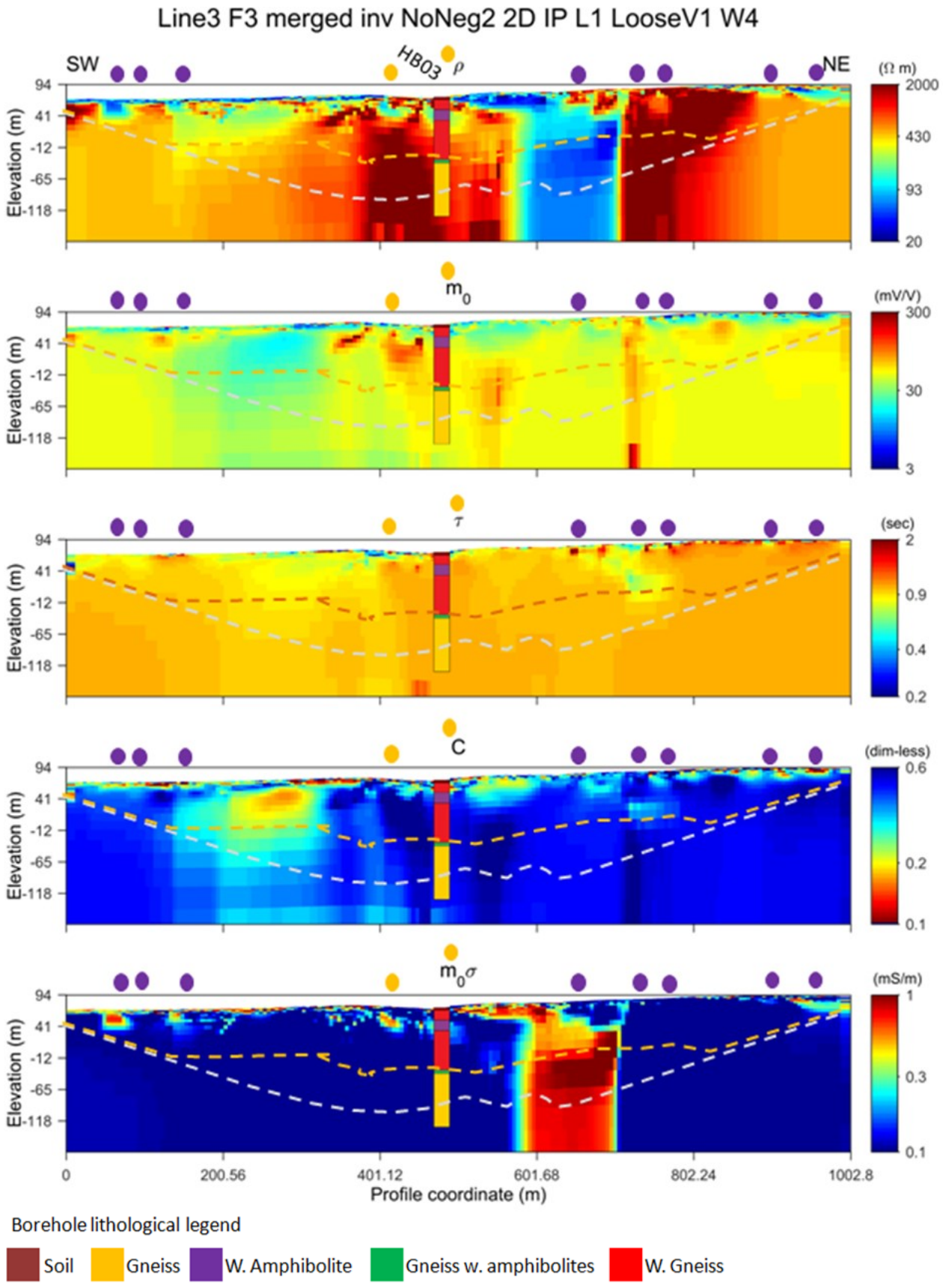

Figure 13. Inverted 2D profile for survey line 3, showing from top to bottom resistivity, IP response, τ, C and normalised IP. Purple and yellow points are magnetic results showing strong or weak anomalies. The borehole HB03 is marked with simplified lithology. The grey dashed line shows the deepest data points and the orange dashed line shows the threshold at which the density of data points is still high.

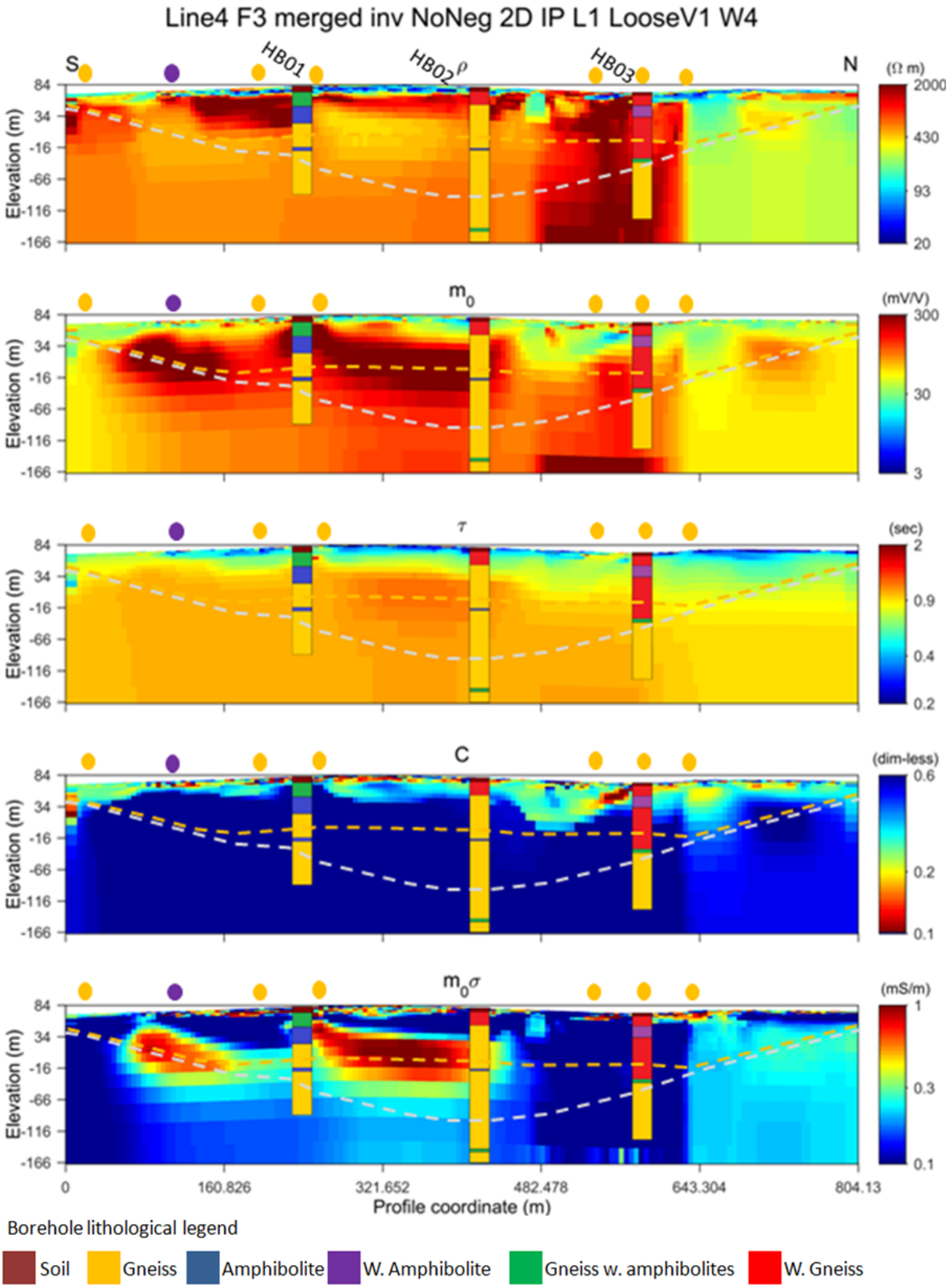

Figure 14. Inverted 2D profile for survey line 4, showing from top to bottom resistivity, IP response, τ, C and normalised IP. Purple and yellow points are magnetic results showing strong or weak anomalies. The boreholes HB01, HB02 and HB03 are marked with simplified lithology. The grey dashed line shows the deepest data points and the orange dashed line shows the threshold at which the density of data points is still high.

5.5 Inversion Result Summary

The figures below (Fig. 15-19) show the profiles together as a grid for each inversion parameter using the program Paraview in order to give a better overview of how differences in the inversions connect between the profiles. In general, the ground has highly varying resistivity and IP response. The resistivity in the ground varies between less than 100 Ωm to over 2000 Ωm. The IP response gives values ranging from zones of 10 mV/V to 300 mV/V. The uppermost layer, varying between 10 and 30 meters, mostly has a low resistivity and IP. In general the bedrock has a high resistivity. Some smaller areas of lower resistivity can be found with a depth up to around 50 m. Also, two larger zones of lower resistivity and IP can be seen. Furthermore, there are some smaller anomalies, especially in the upper parts of the profiles. Both τ and C seem, to some extent, follow the resistivity and IP in terms of high and low zones in the inverted profiles, although not always very clearly. As can be seen when putting the profiles together in a grid, many of the features looks to be linear and stretches in NW-SE direction.

The normalised IP shows two interesting features. The smaller areas of lower resistivity in the upper 50 m have a high normalised IP despite not showing very significant changes in the IP response. Also, the large field of lower resistivity that is present in profile 1-3, has in all three cases a high normalised IP which make them likely to fit together.

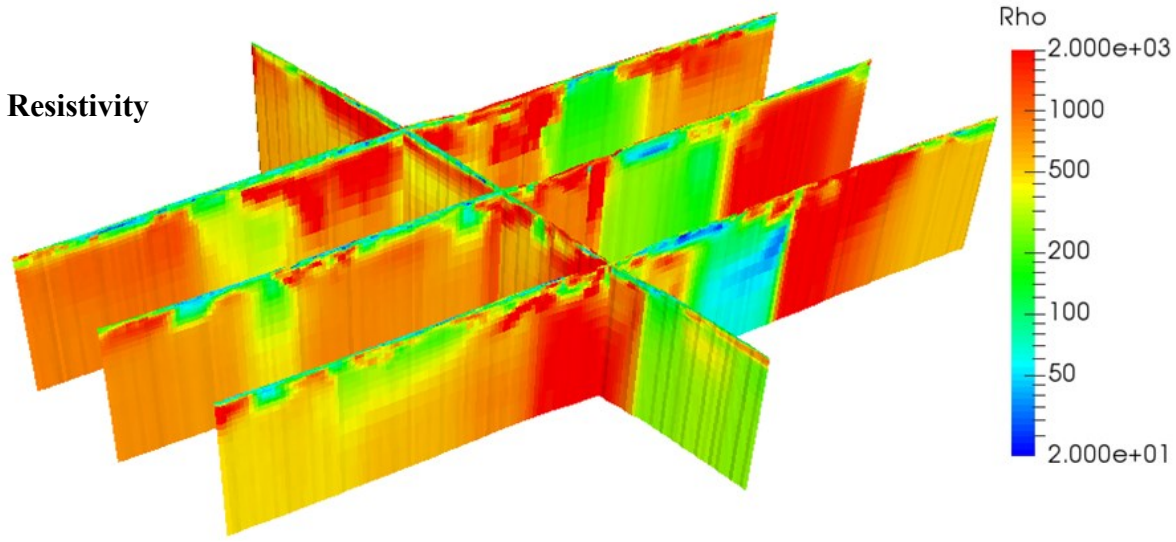

Figure 15. Image showing resistivity for the four profiles together.

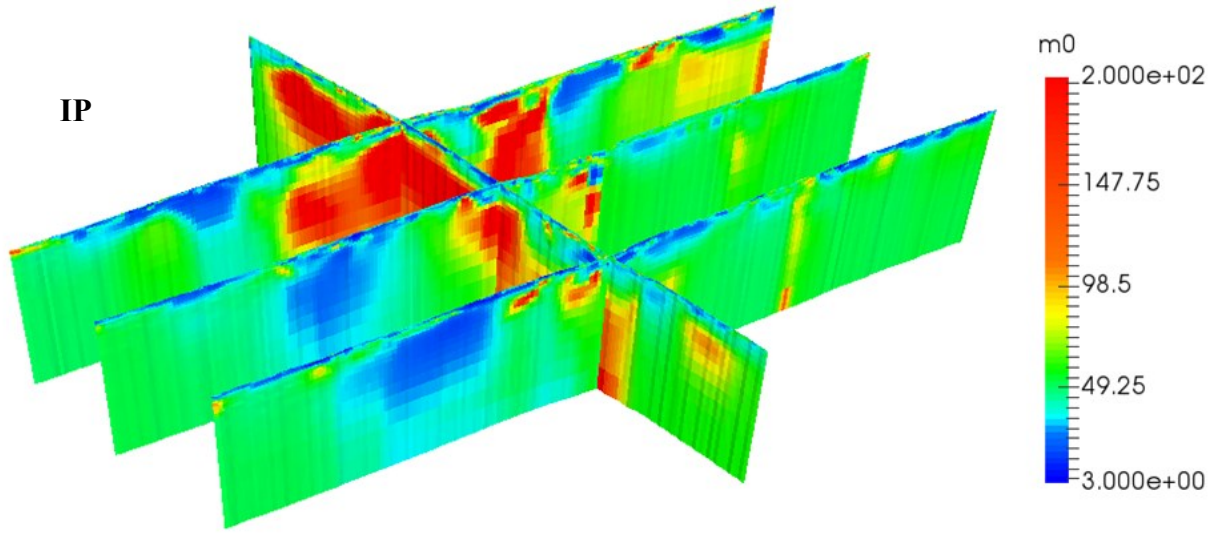

Figure 16. Image showing induced polarization (IP) for the four profiles together.

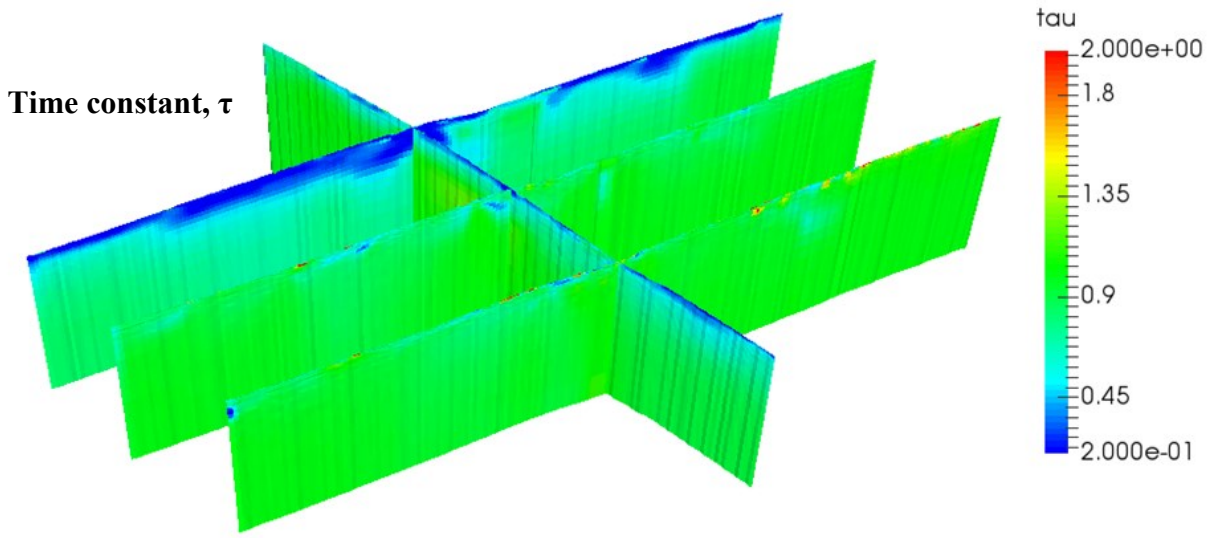

Figure 17. Image showing time constant τ, for the four profiles together.

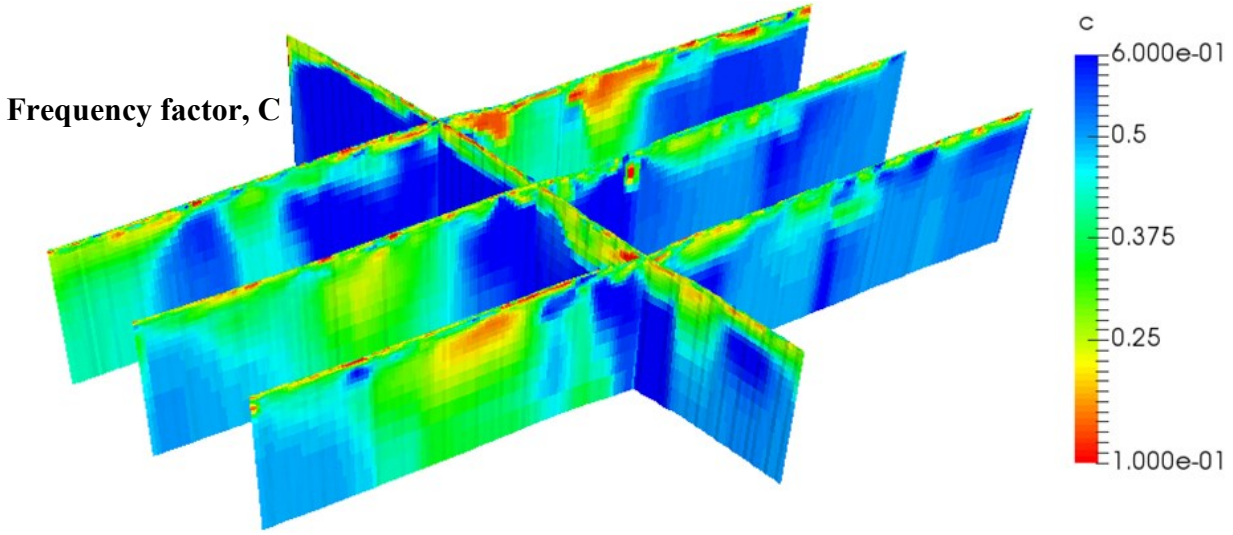

Figure 18. Image showing frequency factor C, for the four profiles together.

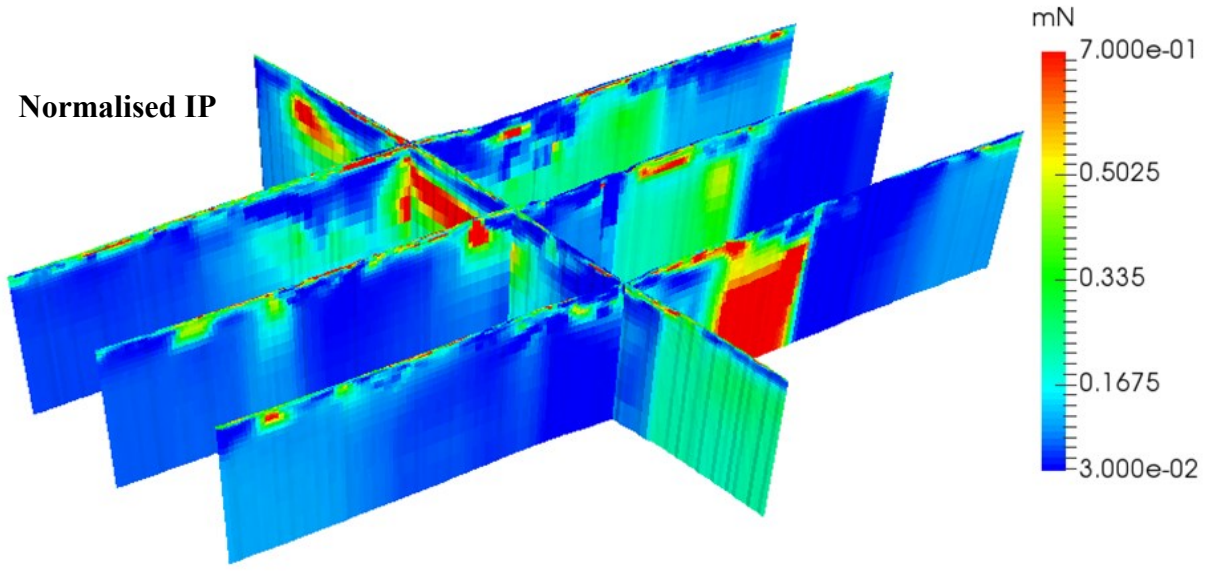

Figur 19. Image showing normalised IP for the four profiles together.

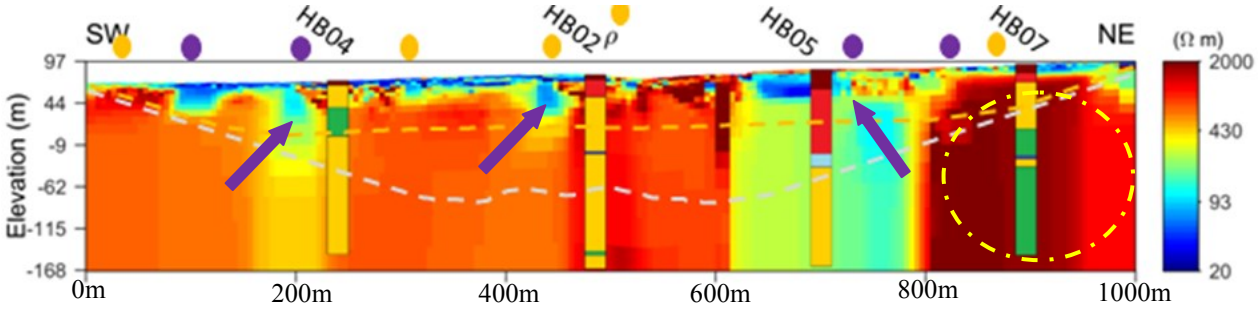

Figure 20. Resistivity profile of profile 2. Purple arrows mark areas with gradual transition, interpreted as weathering and fracture zones. The bedrock surface is marked by a red dashed line where applicable. Yellow dashed circle show relatively intact bedrock, containing numerous amphibolites in the gneiss (green section of the borehole).

5.6 Interpretations

The very upper part of the profiles with varying, but generally lower IP and resistivity, often below 100 Ωm, is interpreted as the soil cover. According to the borehole logs the low resistivity and IP correlate fairly well with what the borehole logs suggest is soil cover, however the transition to higher resistivity is gradual in many cases. The gradual transition is interpreted as zones of more weathered bedrock surface, which also is indicated in several of the borehole logs. The weathered parts are not completely clay altered. However, it is likely that the weathering allows more water to infiltrate, lowering the resistivity. In some cases magnetic anomalies also suggest that there could be dykes or amphibolitisised dykes which could contribute to a more fractured and weathered bedrock in shallow areas. There are also cases where the boundary between soil and bedrock is less distinct. This occurs for example at 250 m and 720 m in profile 1, at 200 m and 700 m in profile 2 and 150 m and 600 m in profile 3. These are all areas with generally lower resistivity. The figure (Fig. 20) below show an example from profile 2 where the areas without clear boundaries are marked out. Other smaller areas of gradual transitions can be found in the centres of the profiles. The interpretation is also strengthened by HB05 and HB03 which report shallow weathering both in lithological and caliper records.

The parts of the profiles that have resistivity values ranging between 1000 Ωm and 2000 Ωm, found especially in the far ends of profile 1-3, are interpreted as relatively intact bedrock mostly made up of gneiss. HB07 shows that especially the deeper parts, in the rightmost area, are mixed with numerous smaller amphibolites as can be seen in Fig. 20. Profile one and three does show somewhat lower resistivities in the deeper and very rightmost parts, but data in these areas are more uncertain since they lack data points and drill data. What can be said is that if the bedrock is the same as in profile two, the amphibolites most likely contribute to the lower values, but are too small to be seen individually. In profile two however, they do not seem to affect the resistivity. The rock is most likely also fractured since the resistivity values at 2000 Ωm are still relatively low for bedrock and fractures are known to be numerous from what can be seen in the Dalby quarry. This interpretation is similar to the classification by Rønning et al. (2013), where these values correspond to fractured water saturated crystalline bedrock.

In several places along the profiles there are areas of lower resistivity going around 50 meters down. These areas have resistivity values often at around 100 Ωm, but without a clear IP anomaly. In several cases they coincide with magnetic indications of dykes or minor magnetic anomalies that could be dykes. This occurs at x=460 m in the very shallow parts of profile 1 and HB01 show some amphibolites at the same depth as the anomaly. In profile 2, the same types of signatures occur at x=110 m and x=200 m. In profile 3, it occurs at x=50 m and x=500 m. In the normalised IP these same areas give a clear elevated normalised IP. They are interpreted as weathering zones, which corresponds with Rønning et al. (2013) where values below 500 Ωm are considered as clay weathering. The normalised IP strengthens this interpretation according to Slater & Lesmes (2002). In HB04, which is situated just next to the area at x=200 m in profile 2, there are numerous amphibolites and some clay in fractures reported between 34 m and 70 m and may contribute to the low resistivity and high normalised IP if they continue to the left in the profile. HB03, situated at the x=500 m anomaly in profile 3 also show shallow weathering and amphibolites in the lithological records and an increase in borehole diameter in the caliper log. In the borehole log, however, the rock is not reported as completely clay altered, therefore, it is probable that some clay has formed but that there are different degrees of weathering or other factors contributing. The areas have probably been intruded by dykes, which have led to increased fracturing and possible local metamorphosis resulting in quicker weathering than the rest of the bedrock. An example of these types of areas in profile 2 is shown below in Fig. 21.

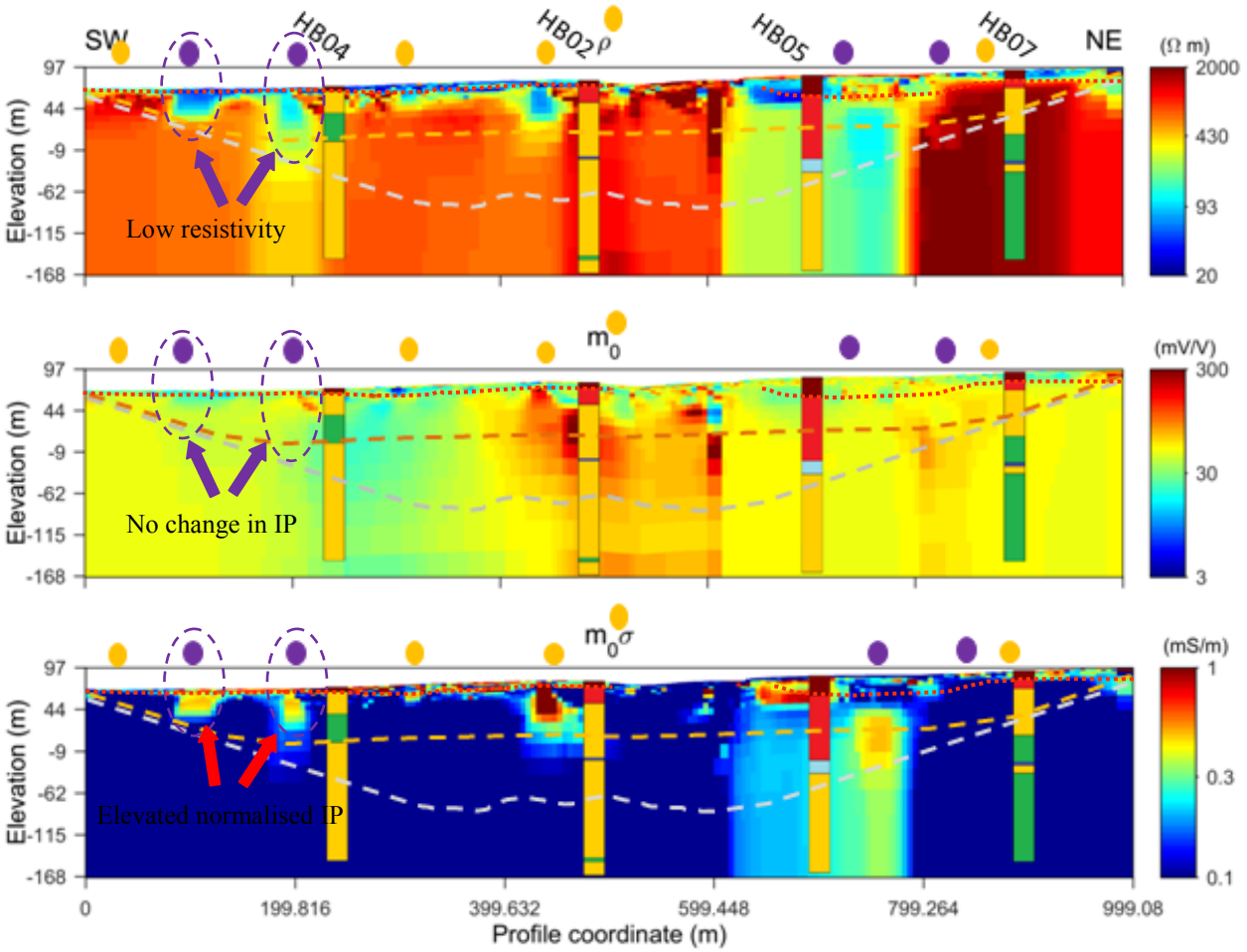

Figure 21. Resistivity, IP and normalised IP for profile 2. Dashed circles and arrows indicate the areas with low resistivity, no IP and elevated normalised IP that correlates with dykes. The red dashed line is the bedrock surface where applicable.

The two larger zones of lower resistivity that can be followed through profiles 1-3, situated at around x=200 m and x=700 m, are similar in both resistivity and IP response. They have lower resistivity and intermediate IP that continues to high depth. However, the area at x=200 m is more noticeable in the upper 100 m. When looking at the normalised IP a clear difference can be seen where the left area shows no, or only very shallow elevated values, whereas the right area on the other hand have a stronger elevation of normalised IP. Dykes are also located in both of these zones. The interpretation of this is that the left area is either a water saturated fracture zone with lower degree of weathering compared to the area at x=700 m, and with weathering not reaching as deep, or that the dyke is more conductive than the surrounding material without giving any clear IP response (Fig 22). Since the area stretches to the right it is possible that not only the dyke has affected the left part of this zone and that the right part of the area is affected by something else, which also gives similar resistivity and IP. The interpretation of the right area is that it is a larger zone of fracturing and weathering, possibly due to the dyke, which would explain the strong normalised IP. This interpretation is strengthened by borehole HB05 which shows weathering down to 107 m and fracture mineralisations below that, and also by the caliper log which shows that the borehole is less stable down to a depth of 105 m. The interpretation also corresponds with classification by Rønning et al. (2013).

In two cases dykes that are giving strong magnetic anomalies also correlate with a vertical IP response but no normalised IP such as at x=820 m in profile 2 and at x=720 m in profile 3. Since profile one lacks this signature, it is possible that inversion effects are contributing, but since similar patterns are seen both in profile two and three, it is likely to be a response to the lithology. This case is interpreted as mostly intact dykes with possible mineralisations due to contact metamorphism or hydrothermal activity in the contact zones (Fig 22). The interpretation would explain the high resistivity and the fact that it gives a higher IP response. This dyke seems to be a possible divider between the weathered zone and the less fractured bedrock with higher resistivity in profile two and three. Also, many of the interpreted dykes give lower resistivity and no or lower IP in this area, except for the case of the rightmost area. According to Cegrell & Mårtensson (2008) the IP should be lower but the resistivity higher. In this case the weathering and high

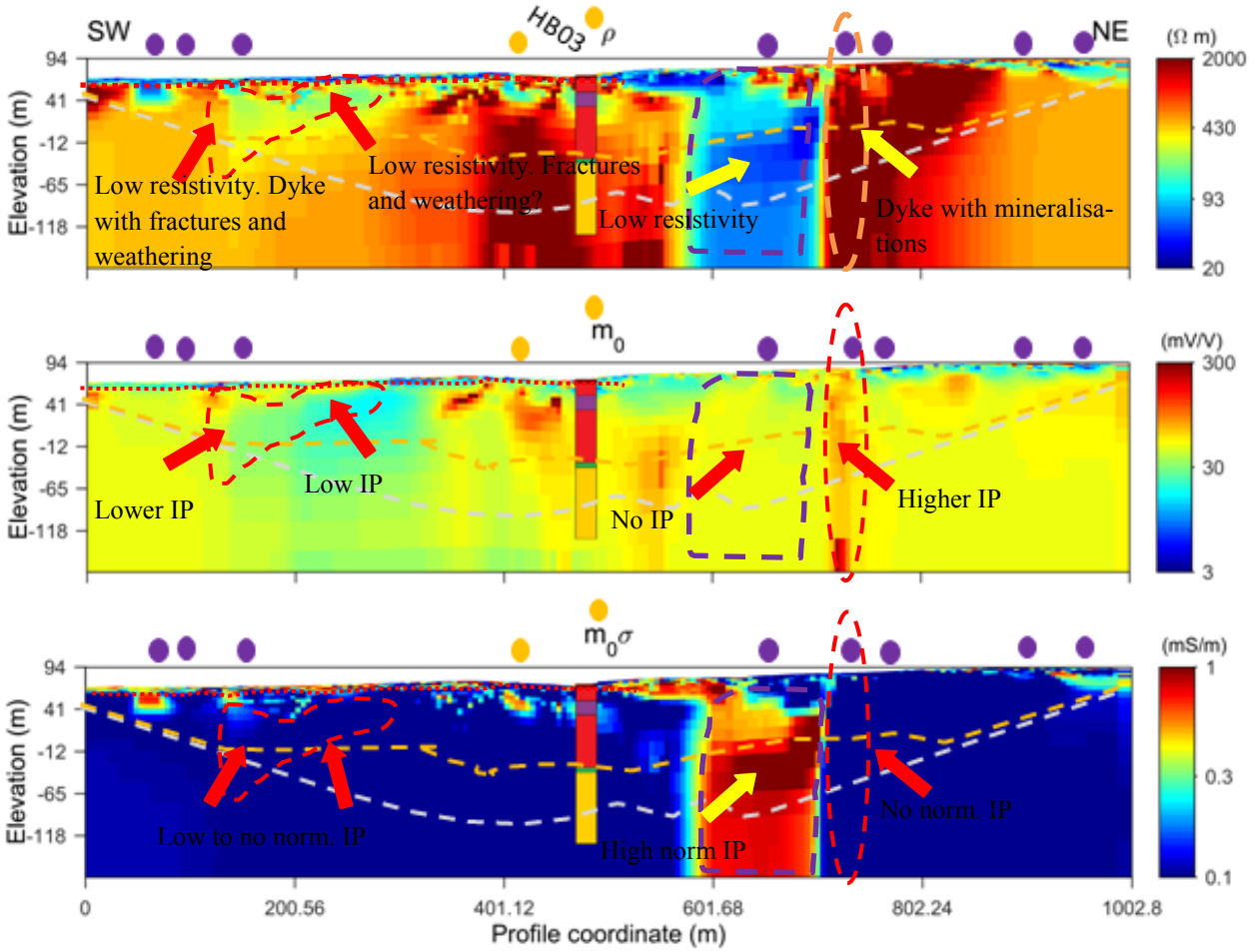

Figure 22. Resistivity, IP and normalised IP for profile 3. The leftmost circled area has low resistivity and IP but no normalised IP. On the right half, two features are shown. The left of them is an area with low resistivity, no IP and high normalised IP. The right has high resistivity, high IP and no normalised IP. Both have dykes coinciding with them.

fracture frequency, that is known in the area could be the cause for the resistivity to be lower instead of higher since it allows the rock to contain more water.

In the centre of profile one, a strong IP anomaly can be seen that decreases towards profile three (Fig 23). It can also be seen in the left part of profile four. The resistivity in this area is relatively high but also decreases towards profile three. Also, the magnetometry does not indicate any clear anomaly in this area. Minor anomalies have been reported, but they seem for the most part, to correlate better with the shallow low resistivity areas. Also, the boreholes situated in this area show some amphibolite in HB01 on profile one, mostly gneiss in HB02 in profile two, and weathered amphibolite and gneiss in HB03 in profile three. The amphibolites in the boreholes and the IP anomaly do not correlate well enough to be the cause of the IP anomaly. It is therefore difficult to determine what this IP anomaly is, however it seems to be an elongated element in the ground going in NW direction.

As for profile four, the bedrock is more even in terms of resistivity (Fig. 24). The resistivity is relatively high until x=640 m where it drops to low values. The only magnetic anomaly is a minor one just at the border between the different resistivity levels, but it is unlikely to be the cause of the change in resistivity. The rock could be more fractured and weathering is increasing to the right in the profile between HB02 and HB03, which could explain the increase in normalised IP and lower resistivity but it is not certain since the area between and to the right of the boreholes is unknown. Since the area is in the end of the profile data coverage is much dense compared to the central part. In the left and centre part of the profile a strong IP and normalised IP areas can be seen. The left area correlate with slightly lower resistivity and a NW trending dyke, which may explain the elongation of the IP area since the dyke in that case would meet profile four in a low angle. However this is not certain since the normalised IP would suggest more weathering than the resistivity does. The same can be seen for the more central IP anomaly except in this are no dyke is reported. The boreholes also show little weathering in the centre of the profile making it more difficult to explain in this study.

As mentioned before the gamma radiation logs from the boreholes are connected to the mineralogy. The radiation is in general higher for red gneiss than for grey gneiss and amphibolite rich horizons vary within the spectrum for the gneisses. The difference

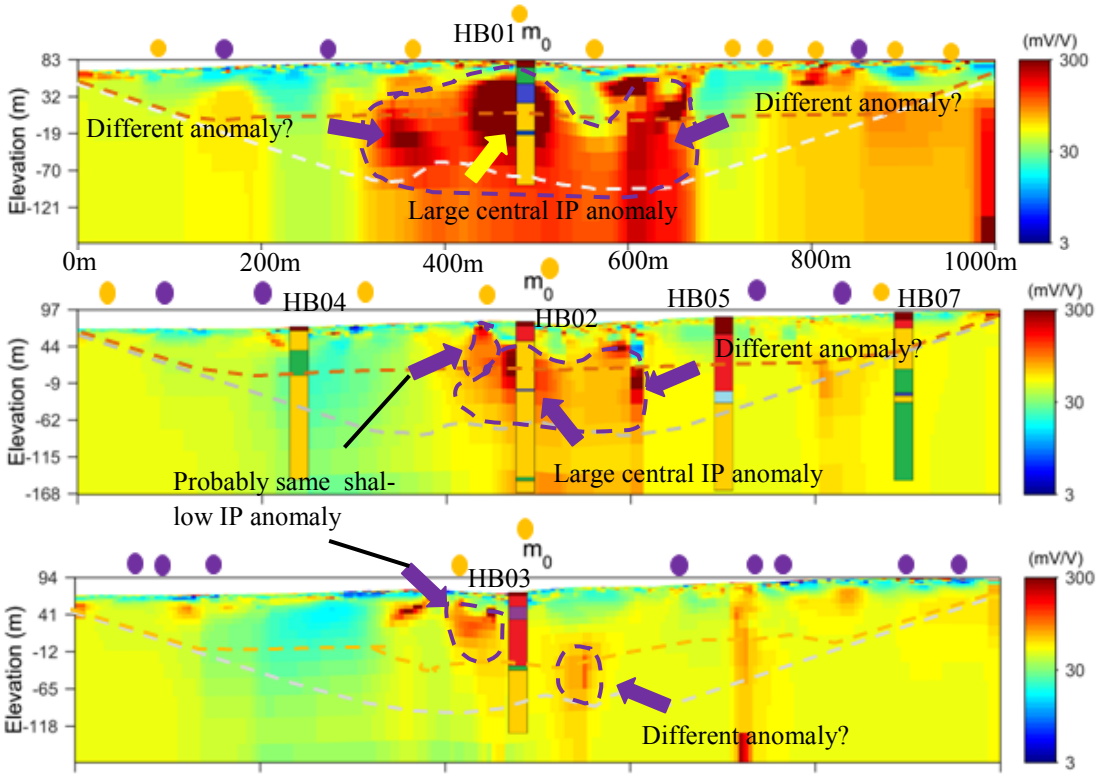

Figure 23. IP sections for profiles 1-3 from top to bottom. The central large IP zone decreases towards profile three and can barely be seen in profile three. the sides of the central IP zone could be individual features. The shallow small IP zones in profile two and three are probably the same feature.

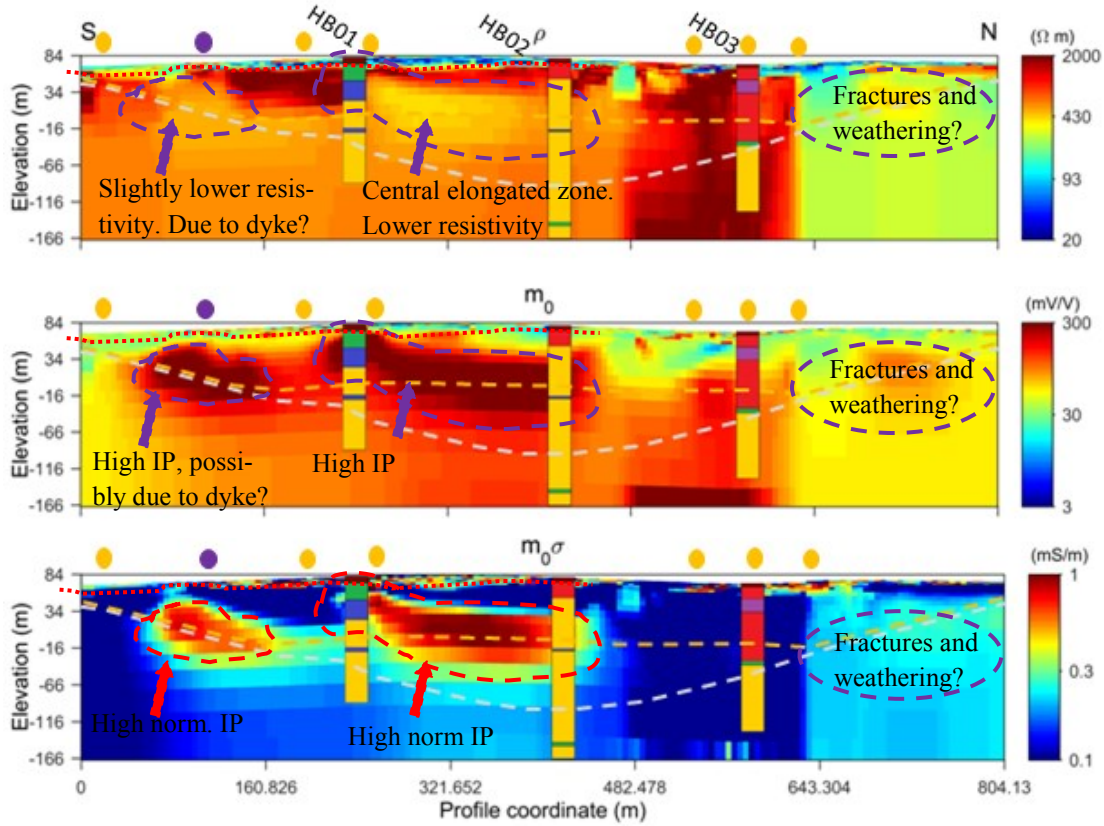

Figure 24. Resistivity, IP and normalised IP for profile 4. In the figure the two elongated areas can be seen with slightly lower resistivity and higher both IP and normalised IP. To the right a larger area of lower resistivity and IP, but with slightly higher normalised IP can be seen.

between the gneisses most likely originate from the amount of K-feldspar, such as the red minerals in gneiss, since it contains potassium K, of which ^{40}K decays to Argon (Ar) and releases gamma rays and to Calcium (Ca) with beta radiation. There may also be differences in Uranium (U) and Thorium (Th) content. However, it is difficult to say within this study how much difference is contributed by potassium relative to the other elements.

To summarise, the bedrock in the area mainly consist of fractured gneiss, some of it weathered to various degree, with numerous NW-SE trending linear elements that are interpreted as dykes, or weakness zones with fractures likely resulting from dykes. Two possible larger weakness zones can be distinguished, one at around x=200 m on the profiles with a dyke and/or a fracture zone and one at around x=700 m with a dyke and larger weathering/fracture zone. The area also contains numerous amphibolitisised dykes trending in NE-SW directions and dipping to the northwest due to deformation. These amphibolitisised dykes probably make the ground in the area generally less stable because they are metamorphosed, deformed and weathered, causing the area in general to have a relatively low resistivity for crystalline rock.

6 Discussion

When looking at the inverted profiles two types of dykes can be seen. One with lower resistivity and high normalised IP due to fracturing and weathering, and one with higher resistivity and no or slightly higher IP, but no normalised IP effect. In the second case it could be that the dyke is not fractured, which would explain the higher resistivity, and in the cases of slightly higher IP there might be polarisable mineralisations in the contact zones.

As can be seen in both the Dalby quarry and the borehole logs the area contains numerous amphibolitisised dykes trending in NE-SW directions and dipping to the northwest. They are often very deformed and weathered varying between a few centimetres to a few meters in width. They may be too small to be clearly distinguished with the 5 meter electrode spacing, with which it is difficult to detect features smaller than 2.5m. It is also increasingly difficult with depth since the number of data points decrease, and overall uncertainties increase. Therefore these dykes most likely contribute to the generally low resistivity and high IP response in the area as well as being a contributing reason for the high fracture occurrence and weathering. The degree of weathering, however, is uncertain as no lithological records from the boreholes have reported complete clay weathering apart from very minor parts. On the other hand, the drilling method used, percussion drilling, only brings up fragments of the ground and will most likely wash away clay, making it more difficult to determine the degree of weathering.

The frequency factor C and the time constant τ both seem to give a lower signature in general where the IP is lower. It's hard to say whether the lower IP is the reason for a lower C and τ or vice versa since the parameters are connected to each other. The lower C would mean that the material has a lower frequency peak, possibly due to several polarization processes and the lower τ would mean that the decay is more rapid which could be connected to smaller polarization length scales, for example fine grained rocks, small pores or clay particles. In the larger weathering zone around 700 m, τ and C are slightly lower which could be contributed to the weathering that is expected here with more size fractions and smaller polarization length scales. The dyke and/or weathering at around 200 m give a similar response, however in profiles two and three the same area is wider and goes into zone 3 which is thought to be less fractured and weathered. It is, therefore, possible that there are textural changes in the ground that is not clearly detected with the resistivity and IP, but which can be seen in the spectral parameters.

In the upper layer of profile one, and to some extent profile four τ is lower than in the same area of the other profiles. This could be due to different properties of the soil, however since most boreholes show a similar soil type with till and clay, it is not certain that this is the reason. It could rather be an inversion effect since the data fit is better for profile one and two compared to profile two and three, which would mean that the latter two show too high τ in this area instead.

In the study area Cole-Cole inversion of DCIP data is able to show where most dykes are situated, however some dykes that can be seen in the magnetometry have not given easily interpretable results in the inverted sections. It is therefore possible that in the cases where they are seen, it is due to the associated fracturing, weathering and possible mineralisations giving interpretable signatures. The bedrock surface is in general easy to detect, apart from in cases where weathering causes a gradual transition to the bedrock in the resistivity values. However, since the soil depth is relatively shallow compared to the investigation depth the resolution makes exact determination of the soil depth difficult. For the same reason, individual fracture zones seem difficult to detect in the study area. When comparing caliper logs with the inverted sections, fracture zones do not show up clearly unless they coincide with an amphibolite zone. This is possibly due to all smaller fractures and weathering that evens out the difference in measurement values, since, in general, the data suggests that few parts are really intact. Another possibility is that resolution issues play a part, evening out the inversion results. Apart from the resolution, most issues seem possible to resolve using a combination of methods.

It has to be said that there are uncertainties in the inversions, and therefore in the interpretations, due to the misfit between data and model that is higher than what is preferred. Many factors could play a part

in this, including the processing of data but also settings in the software cause constraints that the data could not fit. As mentioned before, the early acquisition times were problematic to fit and there are spikes in the misfit sections that were not found during processing. Furthermore, the upper parts of the profiles are usually more trustworthy than the deeper parts since more data is available. The resolution is therefore better which is why the deeper parts should be interpreted with caution. Correlation between the lithology in the boreholes and the geophysical parameters do not always match up well. This is contributed both to the data fit, but also to uncertainties with the drilling method. Despite the uncertainties, the inversions show several linear structures, thought to be dykes, strengthened by magnetometry and weathering zones that are expected in the area and therefore it is probable that at least the major, and shallow, structures are to be trusted. The exact depth and size should however be interpreted with care and smaller, patchier structures, or small areas that have a very sharp difference compared to its surroundings, are more uncertain.

7 Conclusions

- DCIP is useful for characterising the bedrock in Önneslöv. It is concluded that weathered dykes and weathering zones are present and can be found in the area using the method, especially when combining with additional data such as drillings and magnetometry. The bedrock surface can also be seen quite well in most parts, but better resolution could be useful. Dykes interpreted as unweathered are more difficult to detect and need complementary methods, such as magnetometry or drillings.

- The spectral inversion parameters are in this case difficult to interpret. It can however be concluded in this case that lower IP correlates with lower C and τ values and is likely connected to textural differences. More research is needed to better understand how to interpret these parameters and applications of spectral inversion.

- DCIP is in this case good to provide an overview over the bedrock in the area, however on its own there are uncertainties. Drilling is necessary to verify interpretations, but the drilling program may be reduced compared to investigations without DCIP. One limitation with the method used in this study is that the processing of data for spectral inversion at this moment is very time consuming.

- The colour of the gneissic bedrock correlates with the gamma radiation log and is likely connected to the content of K-feldspar minerals.

8 Acknowledgements

I would like to thank my supervisors Torleif Dahlin and Ulf Söderlund for giving me the opportunity to write this thesis, and for their advice along the way. There are also several other people who have contributed in this study. I am very grateful for all the help, and patience, from Per-Ivar Olsson and Sara Johansson, who showed me the software used and gave me advice on how to better process data and interpret results. Also, the fieldwork we did together in Dalby was very educational. I would also like to thank Leif Johansson for tips and help concerning the local geology and Matteo Rossi for interesting discussions. A final thanks is also directed to Lisa Hartmann for proofreading and support along the way.

9 References

Alm, P.,- G., 2012: *"Loggning" Geofysisk Borrhålsmätning*. Compendium. Engineering Geology, Lund University, Lund. 85 pp.

Bergerat, F., Angelier, J., Andreasson, P.,-G., 2007: Evolution of paleostress fields and brittle defor mation of the Tornquist Zone in Scania (Sweden) during Permo-Mesozoic and Cenozo ic times. *Tectonophysics 444*, 93-110.

Bohlin, E. & Landen, L., 2008: *Geofysiska mätmeto der för prospektering till ballastmaterial*. Mas ter thesis, Lund University, Lund, Sweden. 46 pp.

Brander, L. & Söderlund, U., 2009: Mesoprotero zoic (1.47-1.44 Ga) orogenic magmatism in Fennoscandia; Baddeleyite U- Pb dating of a suite of massif-type anorhosite in S. Sweden. *International Journal of Earth Sciences 98*, 499 –516.

Cecys, A., 2004: *Tectonic implications of ca. 1.45 Ga granitoid magmatism at the southwest ern margin of the East European Craton*. Doctoral Thesis, Lund University, Lund, Swe den. 29 pp.

Cederberg, J., 2011: *U-Pb baddelyit dateringar av basiska gångar längs Romeleåsen i Skåne och deras påverkan av plastisk deformation i Pro toginzonen.* Bachelor thesis, Lund University, Lund, Sweden. 16 pp.

Cegrell, M., & Mårtensson, J., 2008: *Resistivity and IP measurements at the Bolmen Tunnel and Ådalsbanan, Sweden*. Master thesis, Lund Uni versity, Lund, Sweden. 37 pp.

Dahlin, T., & Zhou, B., 2006: Multiple-gradient array measurements for multichannel 2D resistivity imaging. *Near Surface Geophysics 4*, 113-123.

Dahlin, T. & Leroux V., 2012: Improvement in time-domain induced polarization data quality with multi-electrode systems by separating current and potential cables. *Near Surface Geophysics 10*, 545-565.

Fiandaca, G., Ramm, J., Binley, A., Gazoty, A., Christiansen, a. V., & Auken, E., 2012: Resolving spectral information from time domain induced polarization data through 2-D inversion. *Geophysical Journal International 192(2)*, 631–646.

Gaál, G., & Gorbatschev, R., 1987: An Outline of the Precambrian Evolution of the Baltic Shield. *Precambrian research 35*, 15-52.

Geotomo Software 2015: Res2dinv_guide 12 pp, Res2dinvx64, 129 pp. Electronic publication reachable at: *http://www.geotomosoft.com/downloads.php*

Gorbatschev, R., 1980: The Precambrian development of southern Sweden. *GFF 102*, 129-136.

Halling, J., 2015: *Inventering av sprickmineraliseringar i en del av Sorgenfrei- Tornquist zonen, Dalby stenbrott, Skåne.* Bachelor thesis, Lund University, Lund, Sweden. 37 pp.

Hubbard, F.H., 1975: The Precambrian crystalline complex of south-western Sweden. The geology and petrogenetic development of the Varberg Region, *GFF 97*, 223-236.

Högdahl, K. (Ed.) et al., 2004: The Transscandinavian Igneous Belt (TIB) in Sweden: a review of its character and evolution. Special Paper 37, Geological Survey of Finland, Espoo.

Johansson, S., 2016: *From microstructure to subsurface characterization: Spectral information from field scale time domain induced polarization*. Licentiate thesis, Lund University, Lund, Sweden. 56 pp.

Johansson, S., Sparrenbom, C., Fiandaca, G., Lindskog, A., Olsson P.I, Dahlin, T. and Rosqvist, H., 2016: Investigations of a Cretaceous limestone with spectral induced polarization and scanning electron microscopy. *Geophysical Journal International* (submitted for publication). 21 pp.

Johansson, L., Lindh, A., Möller, C., 1991: Late Sveconorwegian (Grenville) high-pressure granulite facies metamorphism in southwest Sweden. *Journal of metamorphic Geology, 9*, 283-292.

Klingspor, I., 1976: Radiometric age-determination of basalts, dolerites and related syenite in Skåne, southern Sweden. *Geologiska Föreningen i Stockholm Förhandlingar, 98:3*, 195-216.

Loke, M., H., Acworth, I., Dahlin, T., 2003: A comparison of smooth and blocky inversion methods in 2D electrical imaging surveys. *Exploration Geophysics 34*. 182-187.

Magnusson, K., M., Fernlund, J., M., R., Dahlin, T., 2010: Geoelectrical imaging in the interpretation of geological conditions affecting quarry operations. *Bulletin of Engineering Geology and the Environment, 69*, 465-486.

Möller, A., O'Brien, P., J., Kennedy, A., Kröner, A., 2002: Polyphase zircon in ultrahigh- temperature granulites (Rogaland, SW Norway): Constraints for Pb diffusion in Zircon. *Journal of metamorphic Geology 20*, 727-740.

Norling, E. & Bergström, J., 1986: Mesozoic and Cenozoic tectonic evolution of Scania, southern Sweden. *Tectonophysics, 37*, 7-19.

Olsson, P.-I., Dahlin, T., Fiandaca, G., Auken, E., 2015 A: Measuring time-domain spectral induced polarization in the on-time: decreasing acquisition time and increasing signal-to-noise ratio. *Journal of Applied Geophysics 123*, 312-321.

Olsson, P-I., Fiandaca, G., Dahlin, T., & Auken, E. 2015 B: Impact of Time-domain IP Pulse Length on Measured Data and Inverted Models. Near Surface Geoscience 2015 - 21st European Meeting of Environmental and Engineering Geophysics. EAGE. DOI: 10.3997/2214-4609.201413755

Olsson, P.-I., Fiandaca, G., Larsen, J.J., Dahlin, T., Auken, E., 2016: Doubling the spectrum of time-domain induced polarization by harmonic de-noising, drift correction, spike removal, tapered gating, and data uncertainty estimation. *Geophysical Journal International* (submitted for publication). 26 pp.

Palacky, G.I., 1987: Resistivity characteristics of geological targets. In: Nabighian, M. (Ed.), *Electromagnetic Methods in Applied Geophysics-Theory*. Society of Exploration Geophysicists, Tulsa, OK, pp. 53– 129.

Pelton et al. 1978: Mineral discrimination and removal of inductive coupling with miltifrequency IP. *Geophysics 43*, 588-609.

Reynolds, J., M., 2011: *An introduction to Applied and Environmental Geophysics, Second Edition.* John Wiley & Sons, Ltd.. 696 pp.

Rønning, J., S., Ganerød, G., I., Dalsegg, E., Reiser, F., 2013: Resistivity mapping as a tool for identification and characterisation of weakness zones in crystalline bedrock: definition and testing of an interpretational model. *Bulletin of Engineering Geology and the Environment, 73*, 1225-1244.

Sharma, P., V., 1997: *Environmental and engineering geophysics.* Cambridge University Press. 475.

Slater, D., L., and Lesmes, D. 2002: IP interpretation in environmental investigations. *Geophysics 67*, 77-88.

Söderlund, U., Möller, C., Andersson, J., Johansson, L., Whitehouse, M., 2002: Zircon geochronology in polymetamorphic gneisses in the Sveconorwegian orogen, SW Sweden: ion microprobe evidence for 1.46–1.42 and 0.98–0.96 Ga reworking. *Precambrian Reasearch 113*, 193-225.

Söderlund, U. & Ask, R., 2006: Mesoproterozoic bimodal magmatism alongthe Protogine Zone, S Sweden: three magmatic pulses at 1.56, 1.22

and 1.205 Ga, and regional implications. *GFF 128:4*, 303-310.

Söderlund, U., 2016, personal communication.

Timmerman, M., J., Heeremans, M., Kirstein, L., A., Larsen, B., T., Spencer-Dunworth, E.-A., Sundvoll, B., 2009: Linking changes in tectonic style with magmatism in northern Europe dur ing the late Carboniferous to latest Permian. *Tectonophysics 473*, 375-390.

Wahlgren, C-H., Cruden, A., R., Stephens, M., B., 1994: Kinematics of a major fan-lie structure in the eastern part of the Sveconorwegianorogen, Baltic Shield, south-central Sweden. *Precam brian research 70*, 67-91

Åkesson, S., 2015: *The application of resistivity and IP-measurements as investigation tools at con taminated sites*. Master thesis, Lund University, Lund, Sweden. 82 pp.

10 Appendix

Appendix I - Misfit Sections

Misfit section for profile one.

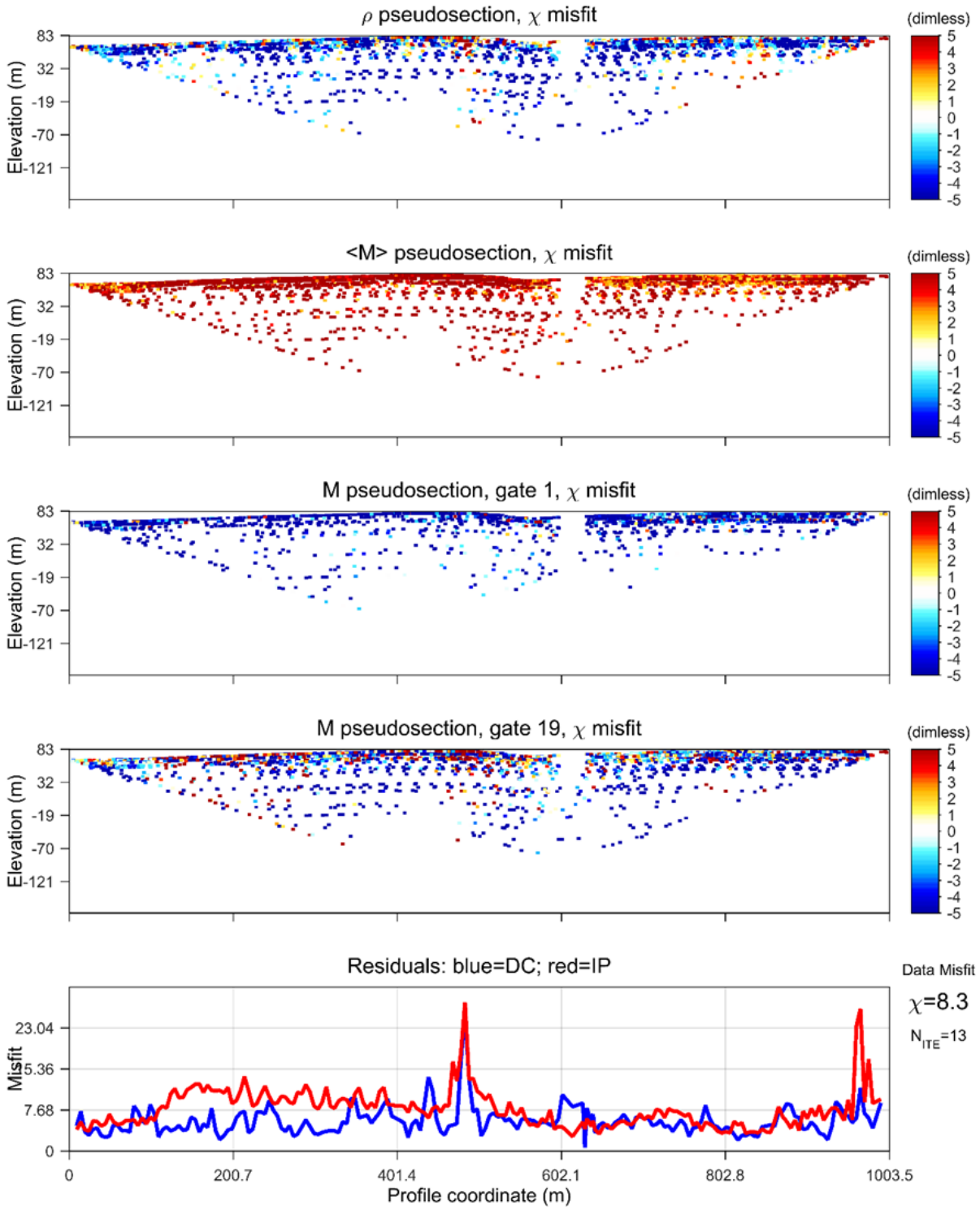

Misfit section for profile two.

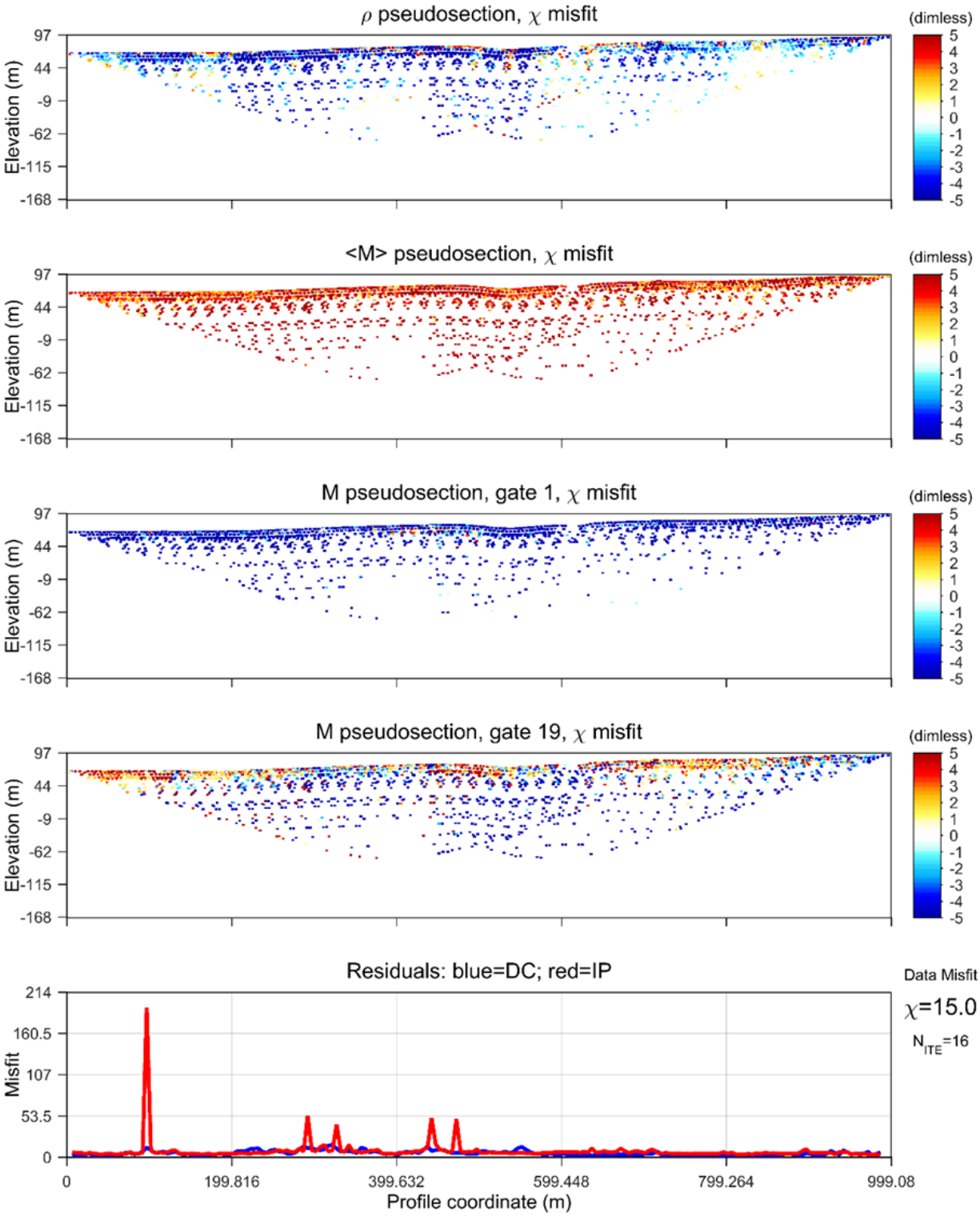

Misfit section for profile three.

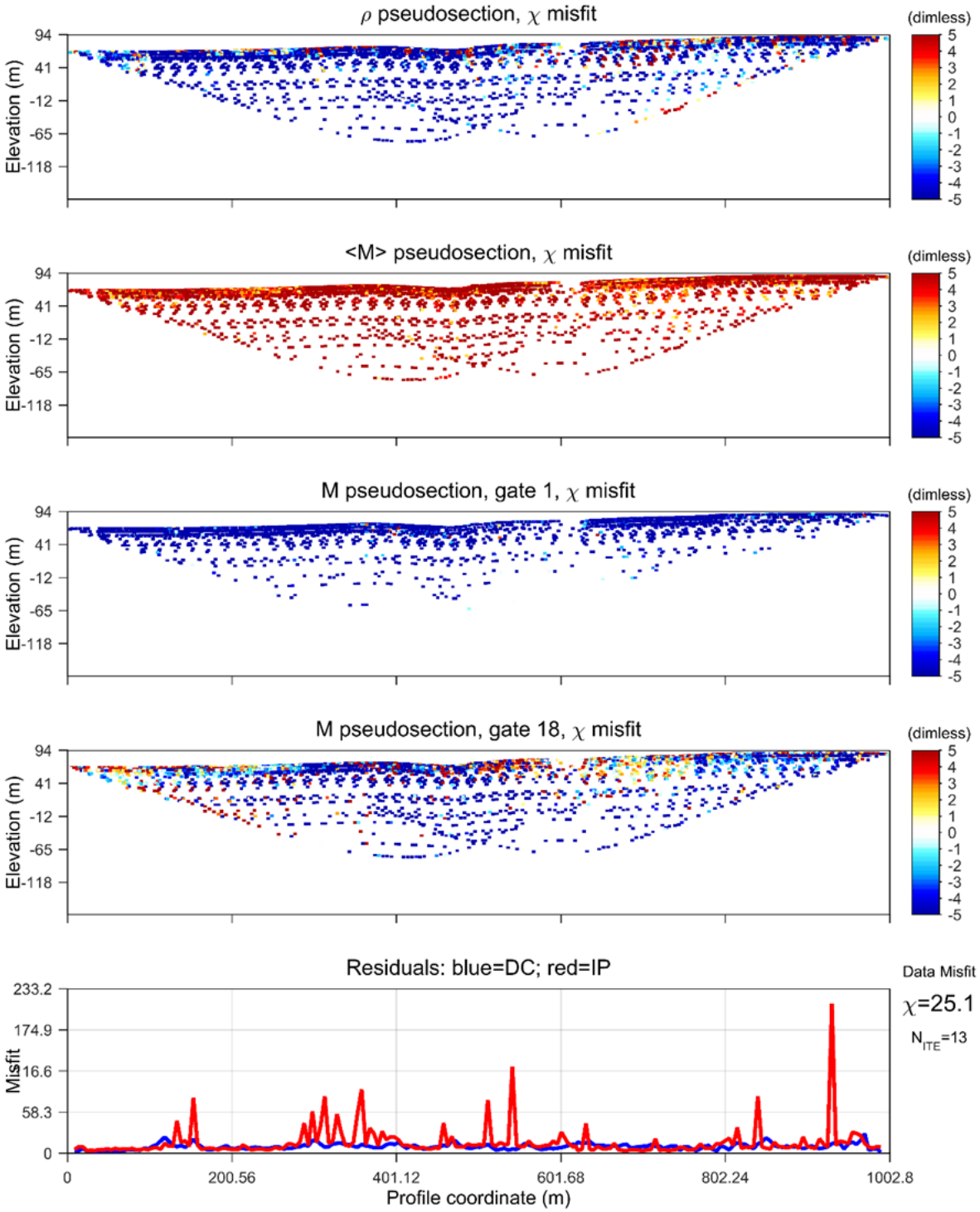

Misfit section for profile four.

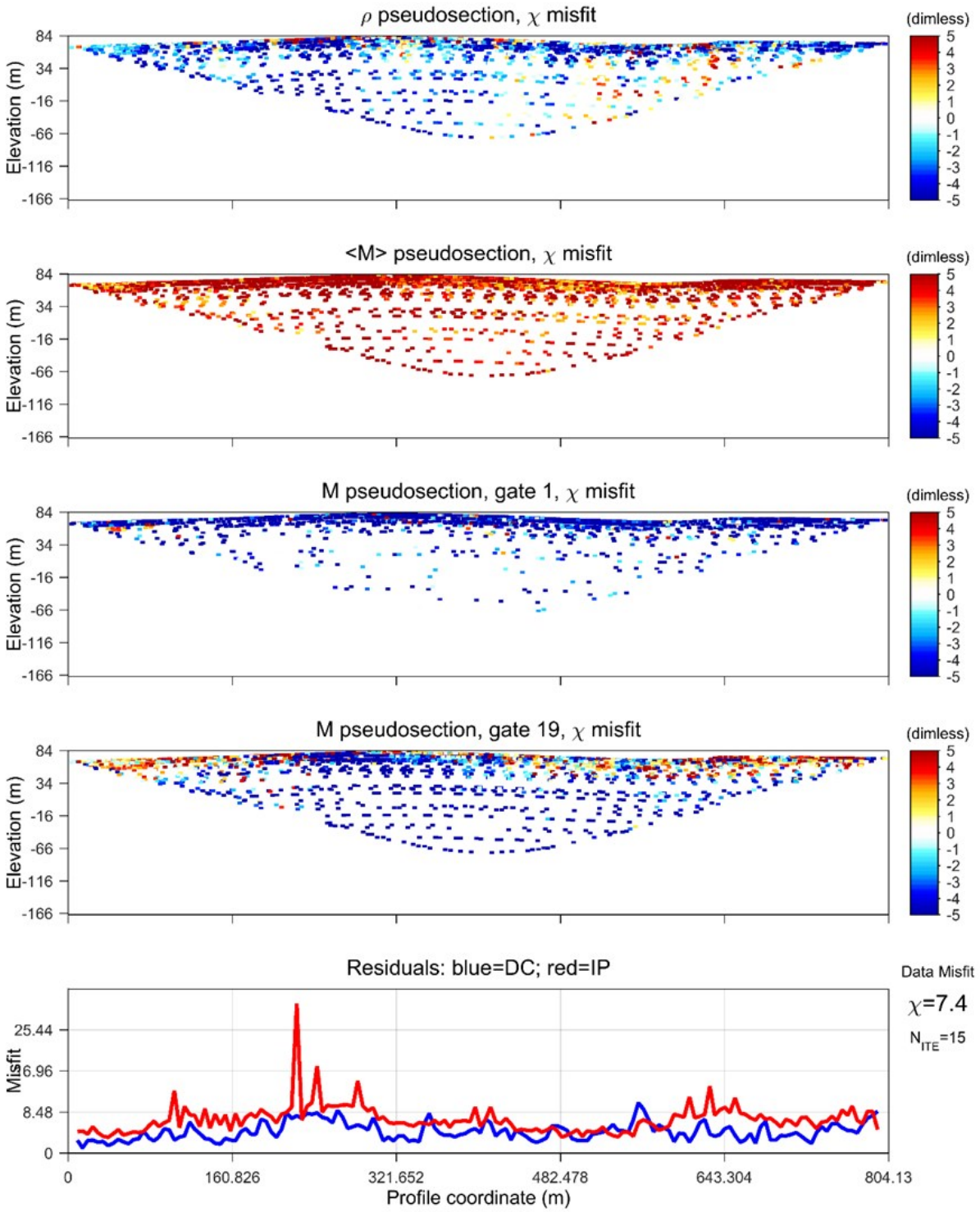

Appendix II - Borehole Logs

Percussion drill log of borehole HB01

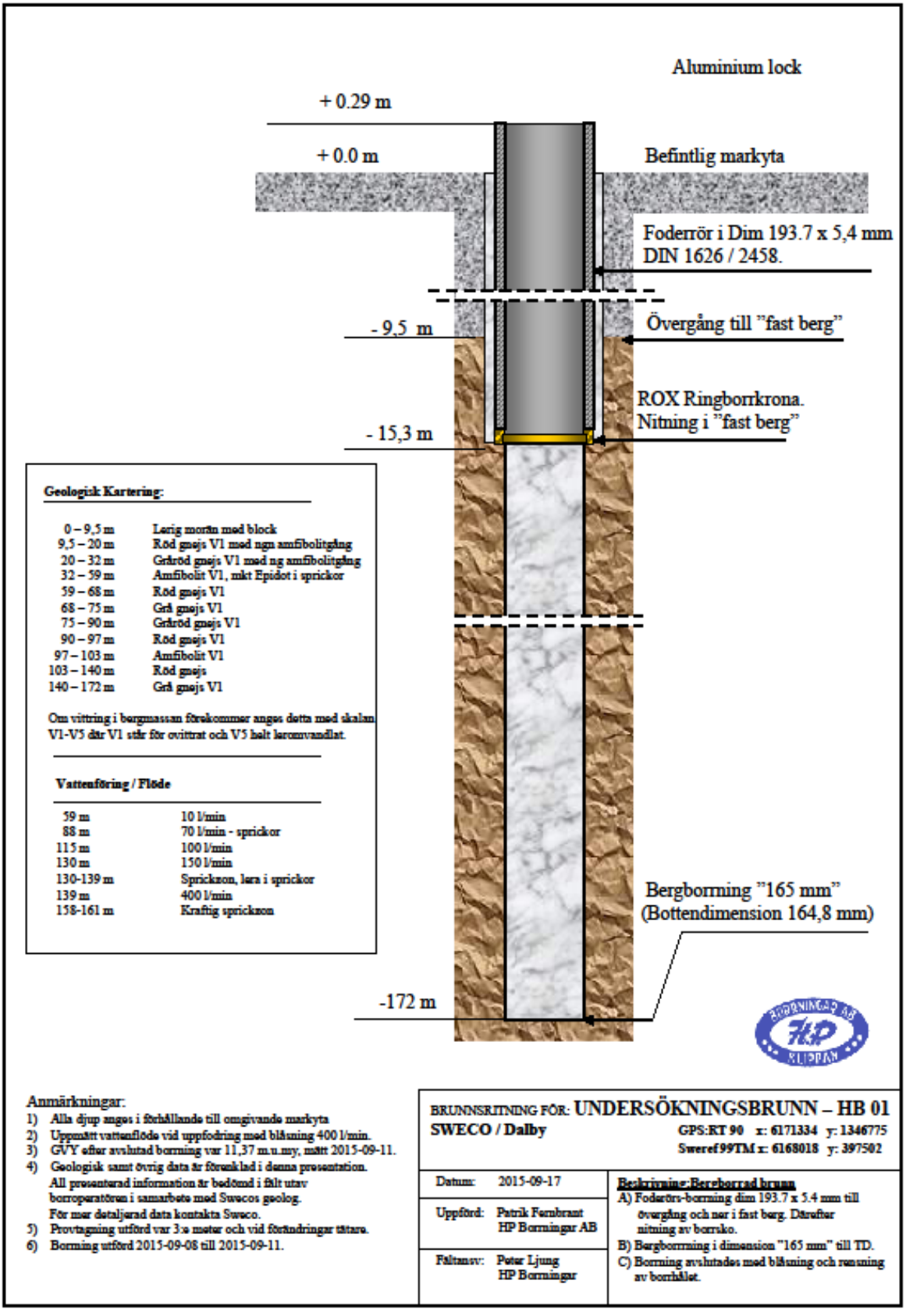

Percussion drill log of borehole HB02

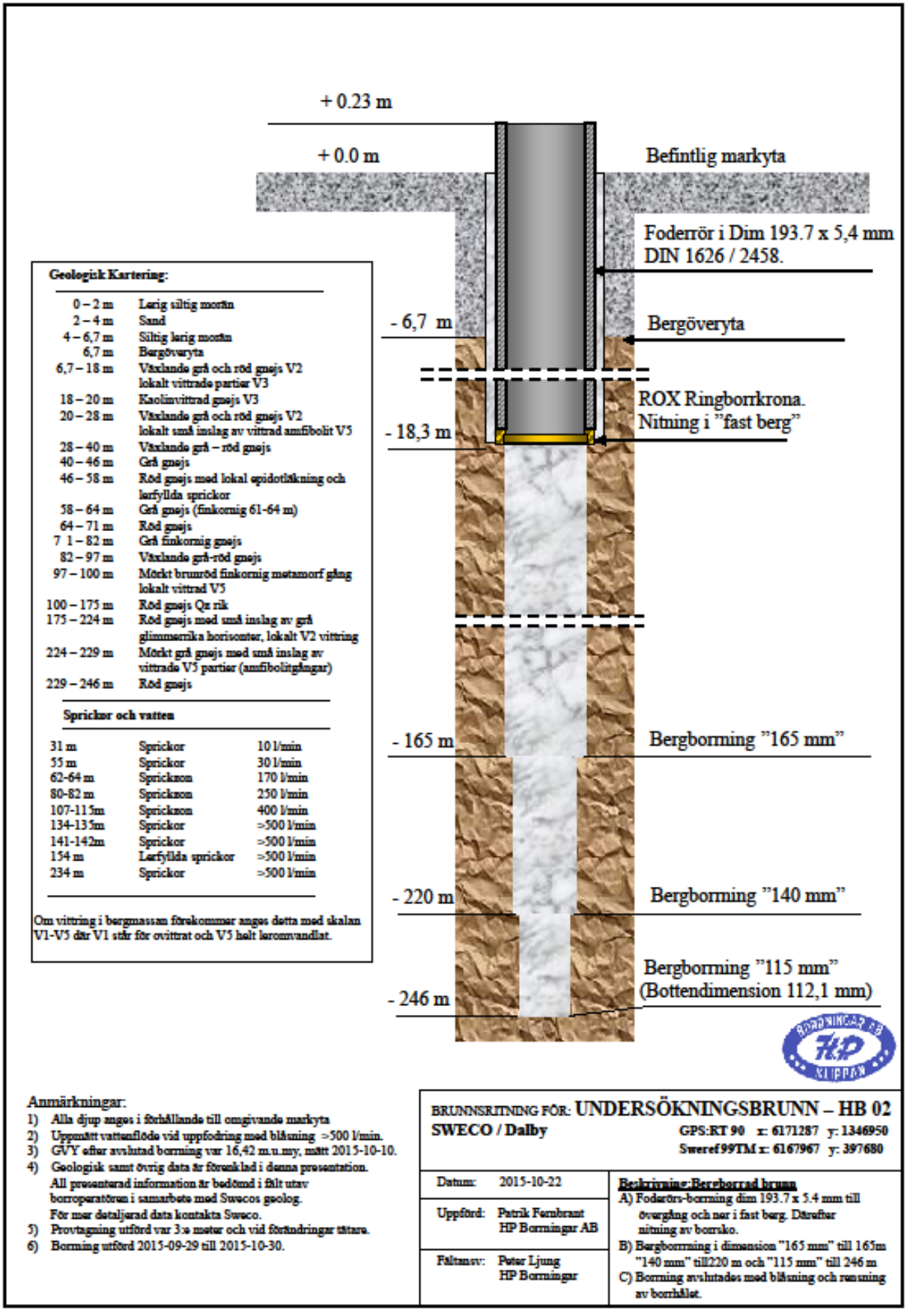

Percussion drill log of borehole HB03

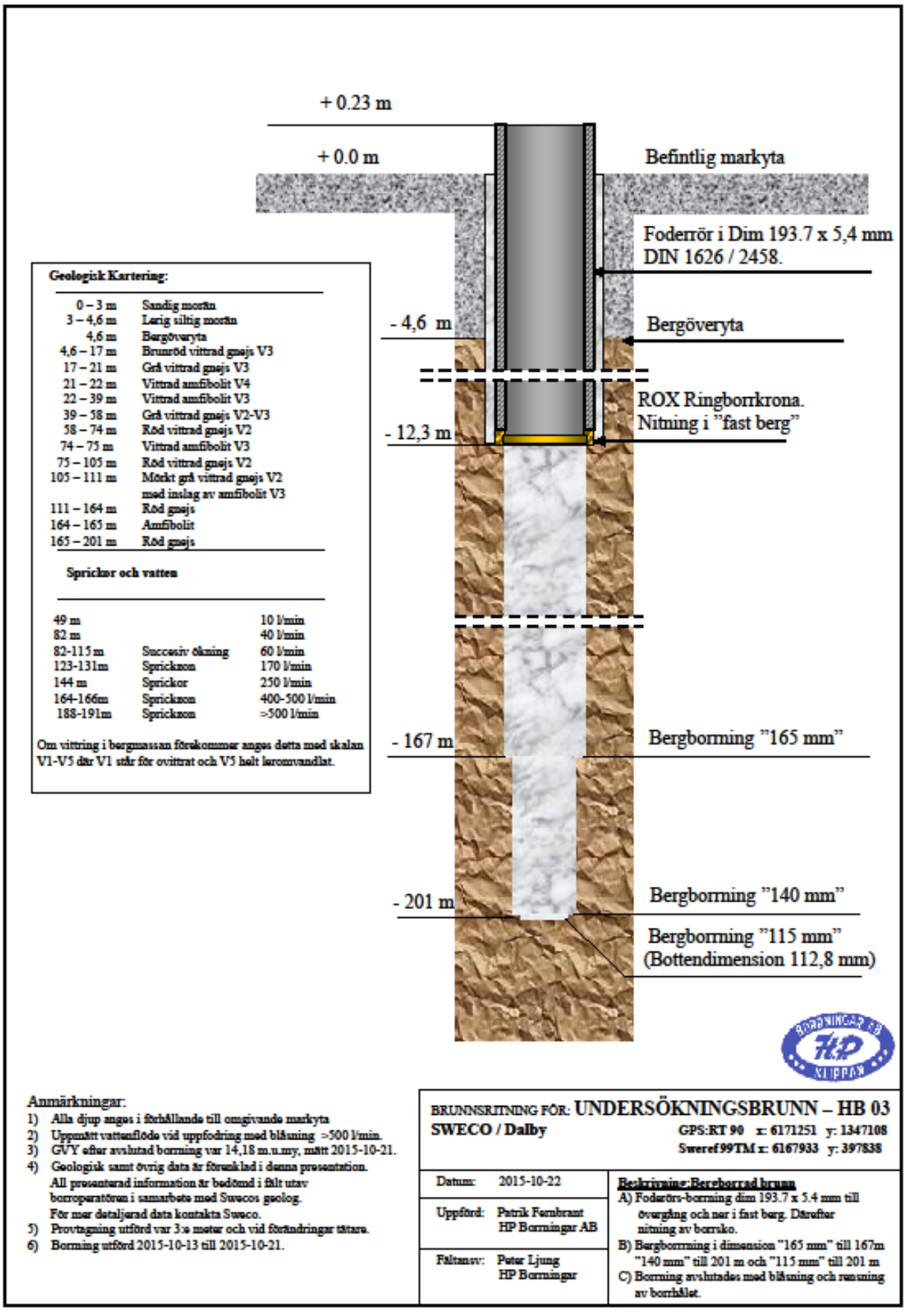

Percussion drill log of borehole HB04

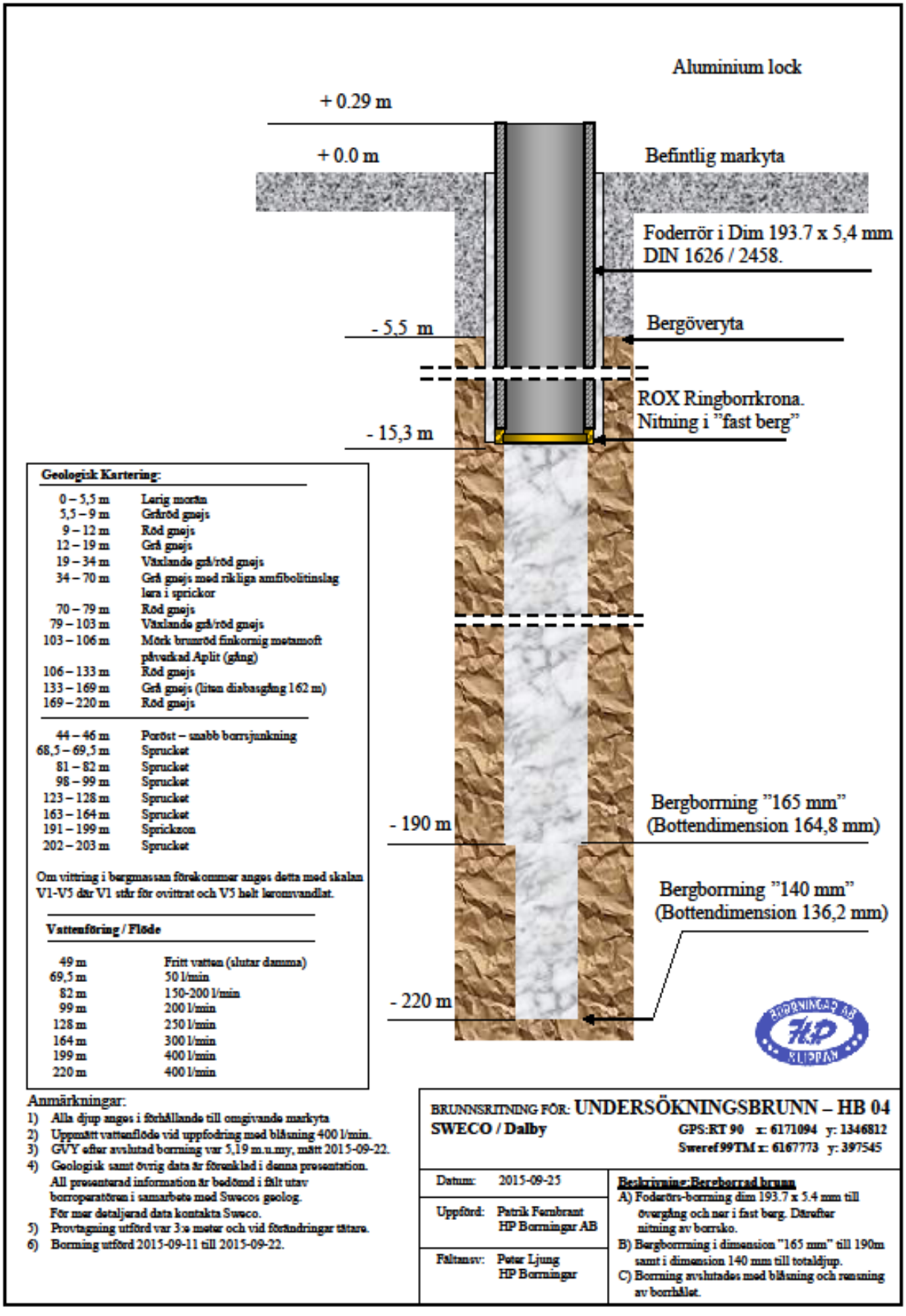

Geologisk Kartering:

0 – 5,5 m	Lerig morän
5,5 – 9 m	Gråröd gnejs
9 – 12 m	Röd gnejs
12 – 19 m	Grå gnejs
19 – 34 m	Växlande grå/röd gnejs
34 – 70 m	Grå gnejs med rikliga amfibolitinslag lera i sprickor
70 – 79 m	Röd gnejs
79 – 103 m	Växlande grå/röd gnejs
103 – 106 m	Mörk brunröd finkornig metamorft påverkad Aplit (gång)
106 – 133 m	Röd gnejs
133 – 169 m	Grå gnejs (liten diabasgång 162 m)
169 – 220 m	Röd gnejs

44 – 46 m	Porös – snabb borrsjunkning
68,5 – 69,5 m	Sprucket
81 – 82 m	Sprucket
98 – 99 m	Sprucket
123 – 128 m	Sprucket
163 – 164 m	Sprucket
191 – 199 m	Sprickzon
202 – 203 m	Sprucket

Om vittring i bergmassan förekommer anges detta med skalan V1-V5 där V1 står för ovittrat och V5 helt leromvandlat.

Vattenföring / Flöde

49 m	Fritt vatten (slutar damma)
69,5 m	50 l/min
82 m	150-200 l/min
99 m	200 l/min
128 m	250 l/min
164 m	300 l/min
199 m	400 l/min
220 m	400 l/min

Anmärkningar:

1) Alla djup anges i förhållande till omgivande markyta
2) Uppmätt vattenflöde vid uppfodring med blåsning 400 l/min.
3) GVY efter avslutad borrning var 5,19 m.u.my, mätt 2015-09-22.
4) Geologisk samt övrig data är förenklad i denna presentation. All presenterad information är bedömd i fält utav borroperatören i samarbete med Swecos geolog. För mer detaljerad data kontakta Sweco.
5) Provtagning utförd var 3:e meter och vid förändringar tätare.
6) Borrning utförd 2015-09-11 till 2015-09-22.

BRUNNSRITNING FÖR: **UNDERSÖKNINGSBRUNN – HB 04**

SWECO / Dalby

GPS:RT 90 x: 6171094 y: 1346812
Sweref 99TM x: 6167773 y: 397545

Datum:	2015-09-25
Uppförd:	Patrik Fernbrant HP Borningar AB
Fältansv:	Peter Ljung HP Borningar

Beskrivning:Bergborrad brunn

A) Foderörs-borrning dim 193.7 x 5.4 mm till övergång och ner i fast berg. Därefter nitning av borrsko.
B) Bergborrning i dimension "165 mm" till 190m samt i dimension 140 mm till totaldjup.
C) Borrning avslutades med blåsning och rensning av borrhålet.

Percussion drill log of borehole HB05

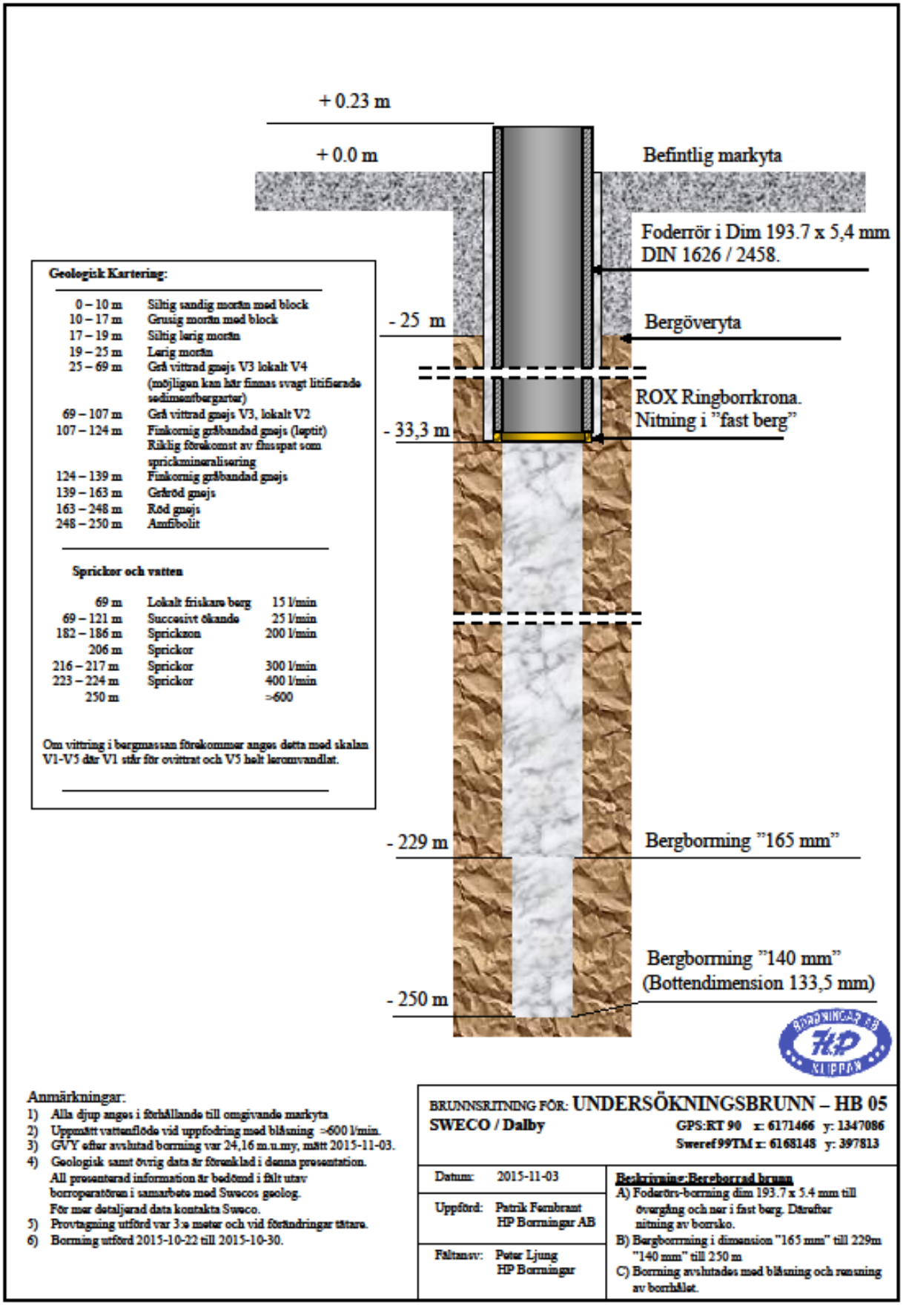

Percussion drill log of borehole HB06

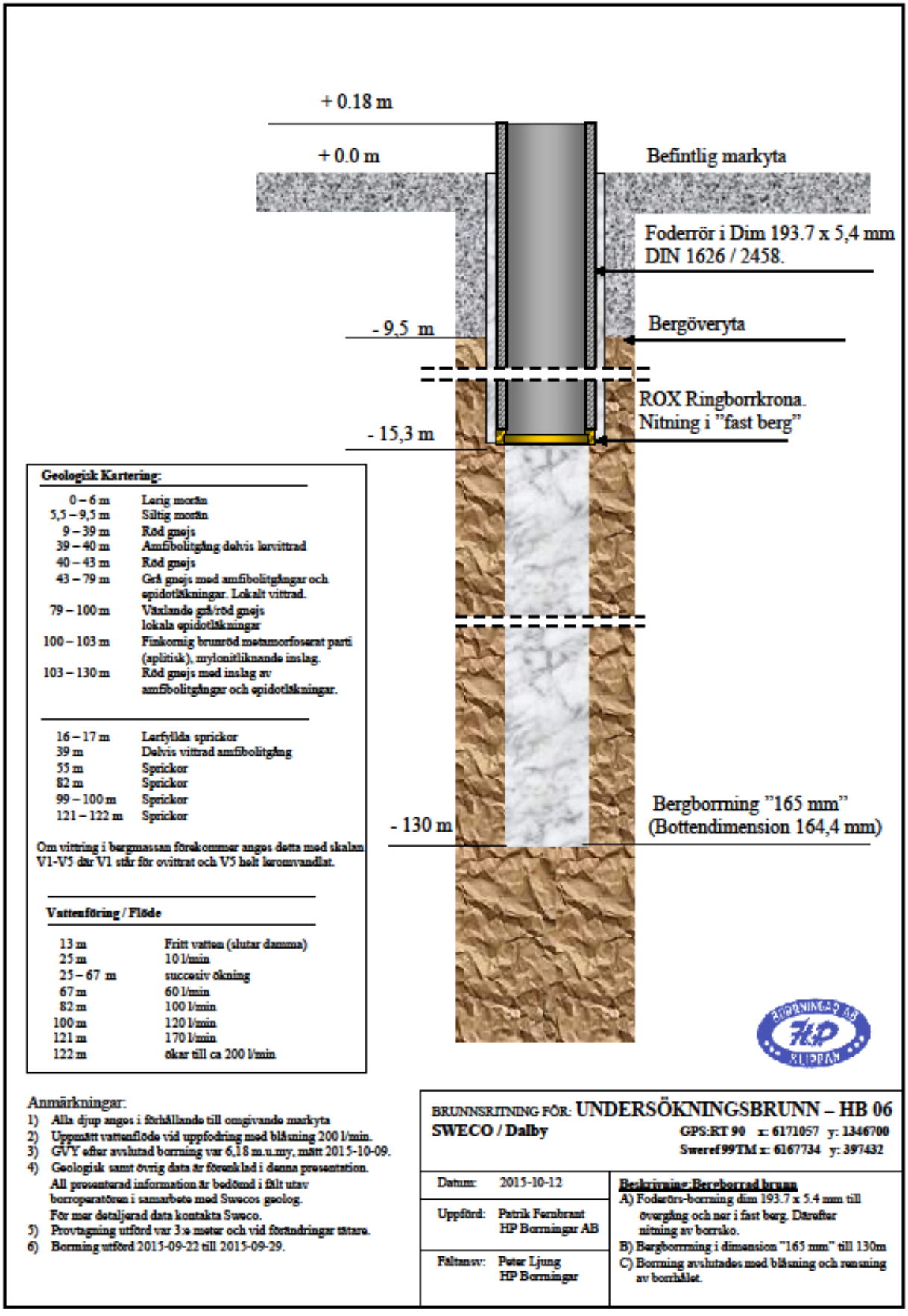

Percussion drill log of borehole HB07

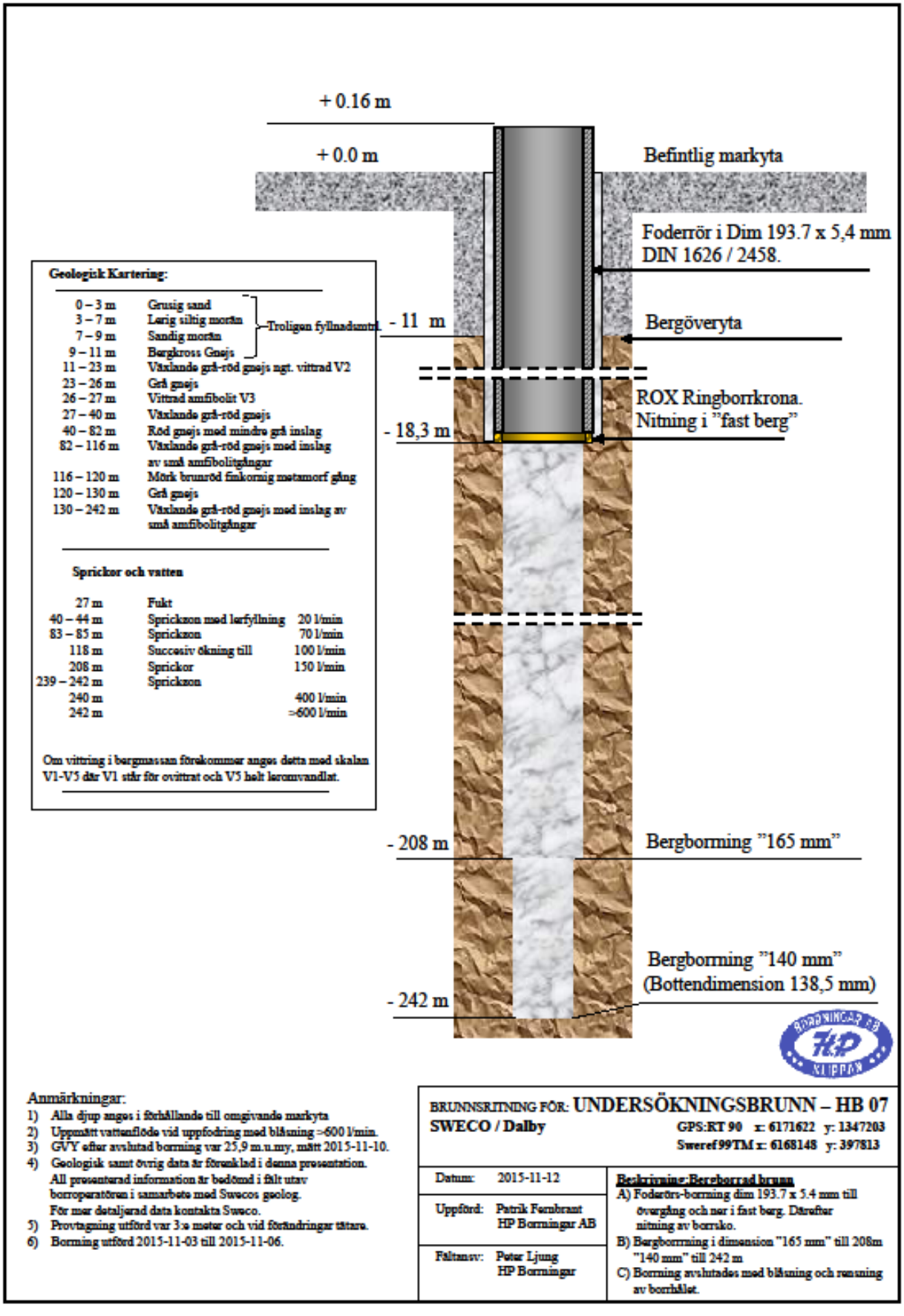

Appendix III - Natural Gamma and Caliper Logs

Natural gamma and caliper log from HB02

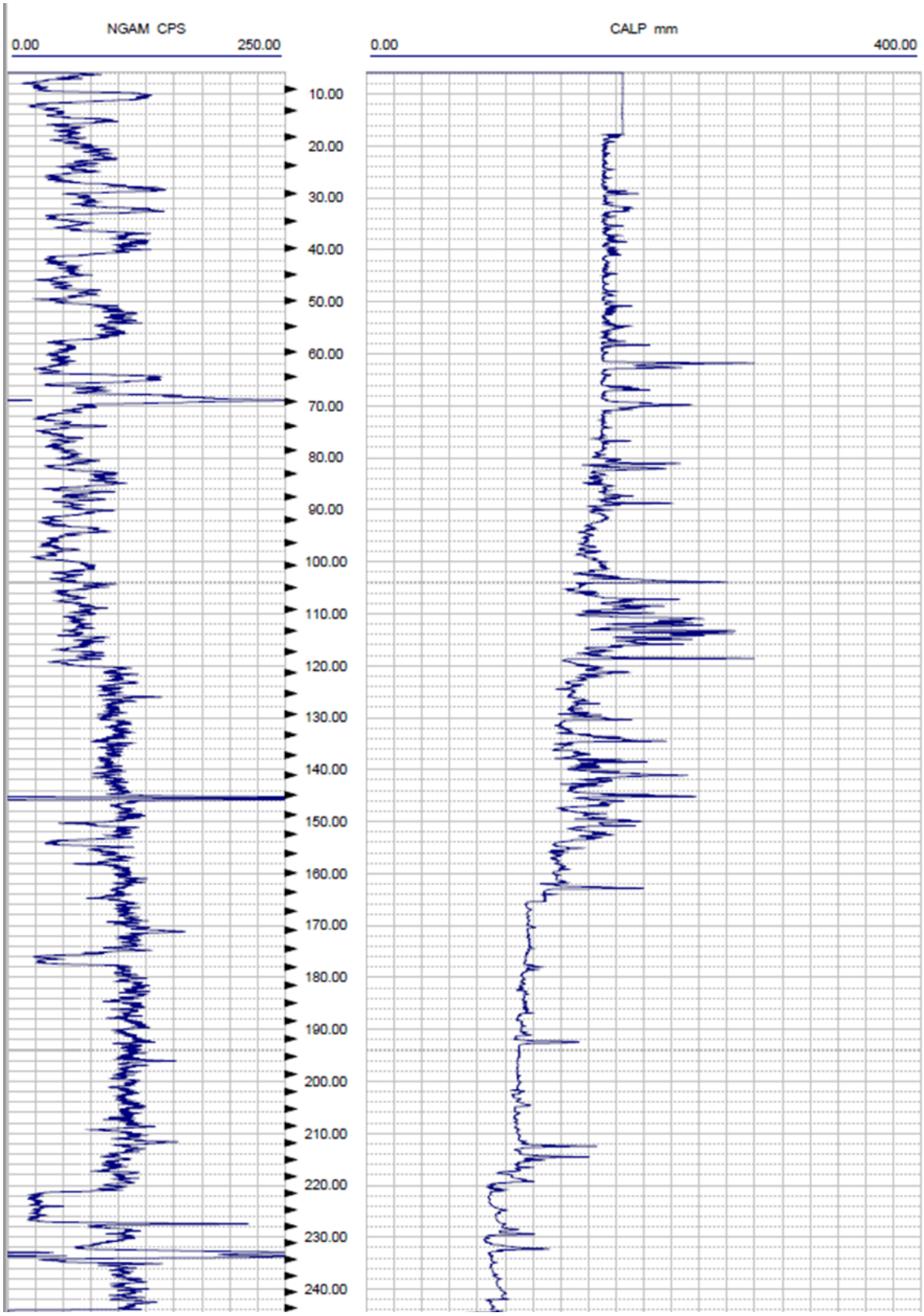

Natural gamma and caliper log from HB03

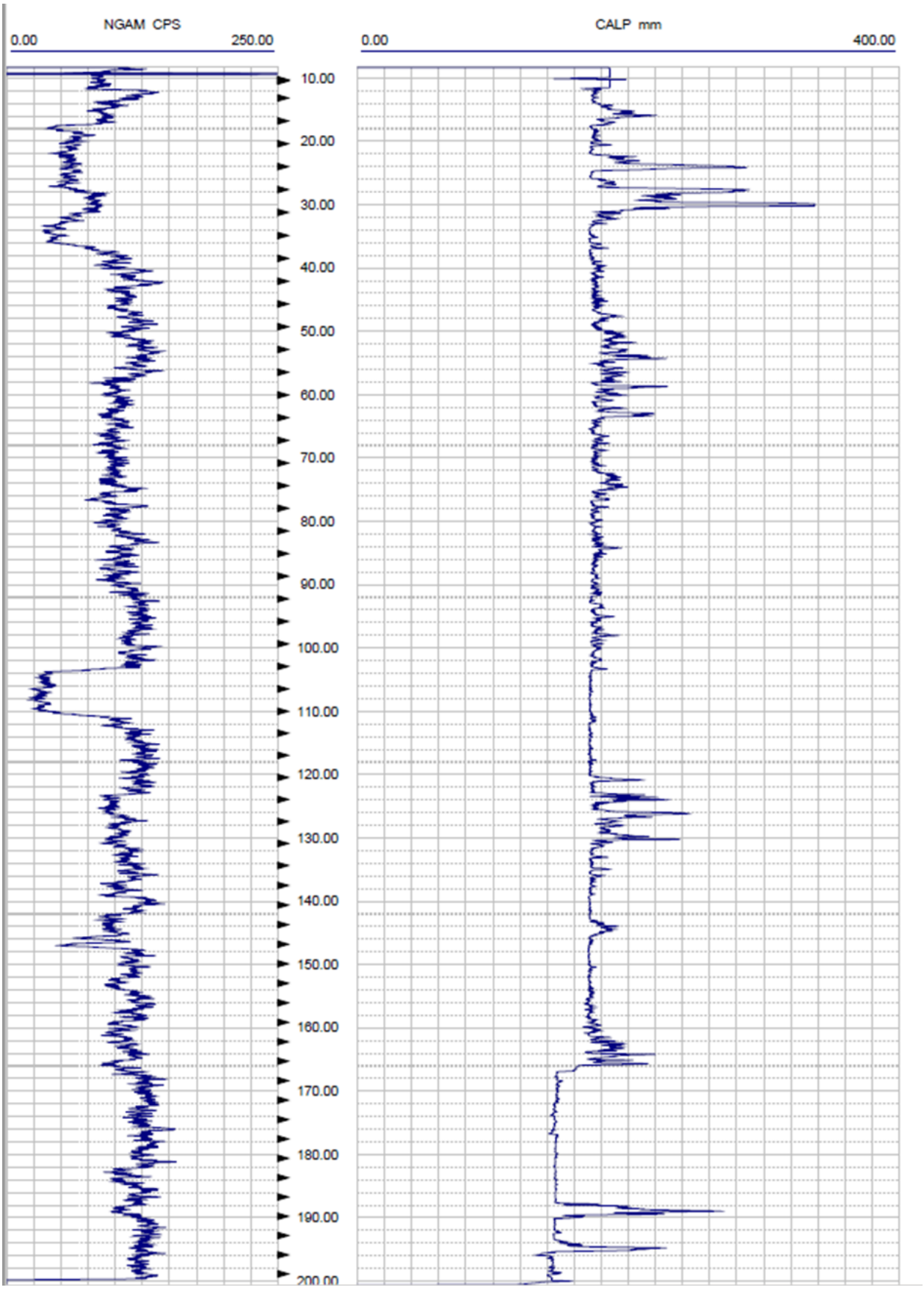

Natural gamma and caliper log from HB05

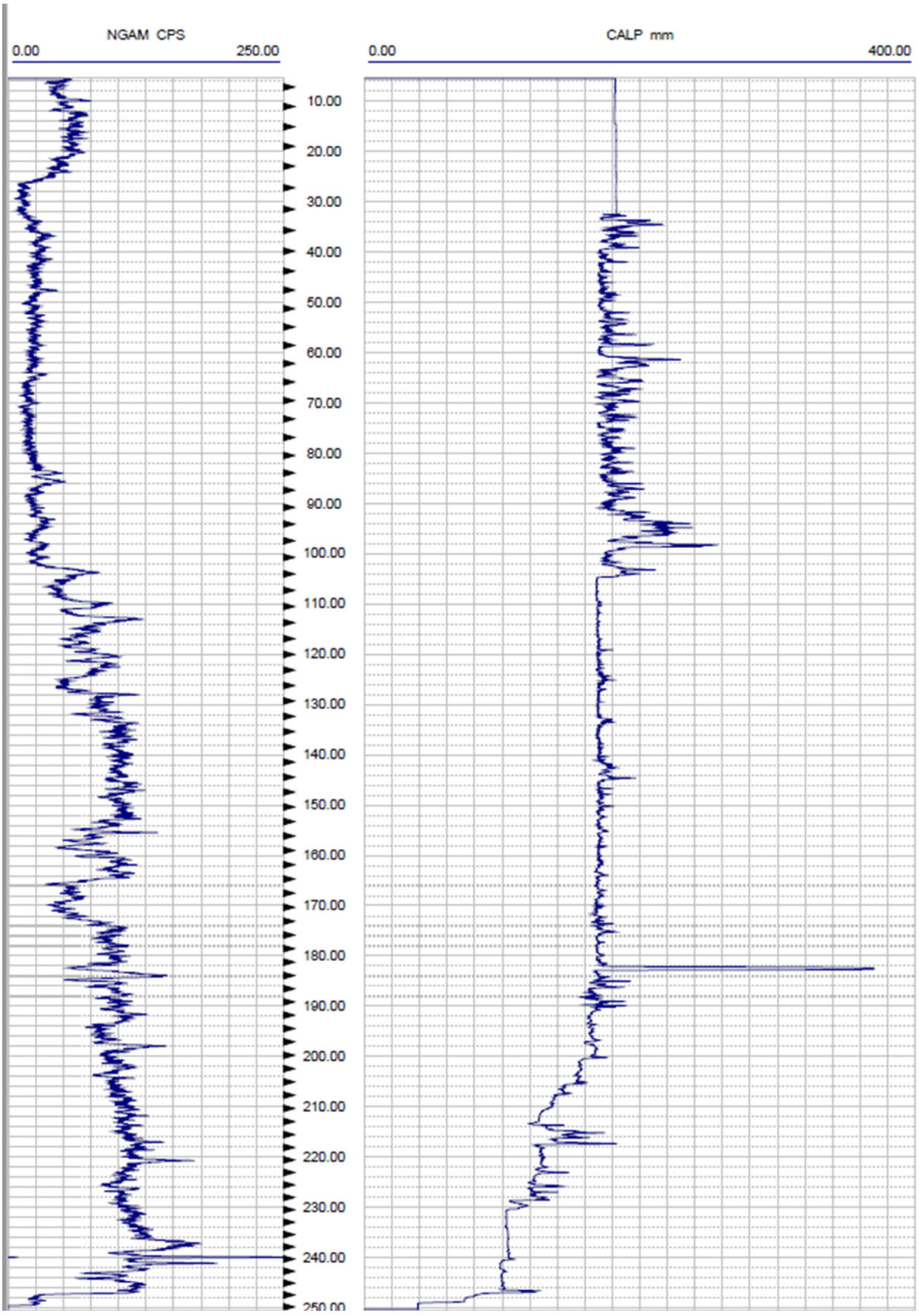

Tidigare skrifter i serien ”Examensarbeten i Geologi vid Lunds universitet”:

441. Holm, Julia, 2015: Markskador inom skogsbruket - jordartens betydelse (15 hp)
442. Åkesson, Sofia, 2015: The application of resistivity and IP-measurements as investigation tools at contaminated sites - A case study from Kv Renen 13, Varberg, SW Sweden. (45 hp)
443. Lönsjö, Emma, 2015: Utbredningen av PFOS i Sverige och världen med fokus på grundvattnet – en litteraturstudie. (15 hp)
444. Asani, Besnik, 2015: A geophysical study of a drumlin in the Åsnen area, Småland, south Sweden. (15 hp)
445. Ohlin, Jeanette, 2015: Riskanalys över pesticidförekomst i enskilda brunnar i Sjöbo kommun. (15 hp)
446. Stevic, Marijana, 2015: Identification and environmental interpretation of microtextures on quartz grains from aeolian sediments - Brattforsheden and Vittskövle, Sweden. (15 hp)
447. Johansson, Ida, 2015: Is there an influence of solar activity on the North Atlantic Oscillation? A literature study of the forcing factors behind the North Atlantic Oscillation. (15 hp)
448. Halling, Jenny, 2015: Inventering av sprickmineraliseringar i en del av Sorgenfrei-Tornquistzonen, Dalby stenbrott, Skåne. (15 hp)
449. Nordas, Johan, 2015: A palynological study across the Ordovician Kinnekulle. (15 hp)
450. Åhlén, Alexandra, 2015: Carbonatites at the Alnö complex, Sweden and along the East African Rift: a literature review. (15 hp)
451. Andersson, Klara, 2015: Undersökning av slugtestsmetodik. (15 hp)
452. Ivarsson, Filip, 2015: Hur bildades Bushveldkomplexet? (15 hp)
453. Glommé, Alexandra, 2015: $^{87}Sr/^{86}Sr$ in plagioclase, evidence for a crustal origin of the Hakefjorden Complex, SW Sweden. (45 hp)
454. Kullberg, Sara, 2015: Using Fe-Ti oxides and trace element analysis to determine crystallization sequence of an anorthosite-norite intrusion, Älgön SW Sweden. (45 hp)
455. Gustafsson, Jon, 2015: När började plattektoniken? Bevis för plattektoniska processer i geologisk tid. (15 hp)
456. Bergqvist, Martina, 2015: Kan Ölands grundvatten öka vid en uppdämning av de utgrävda dikena genom strandvallarna på Ölands östkust? (15 hp)
457. Larsson, Emilie, 2015: U-Pb baddeleyite dating of intrusions in the south-easternmost Kaapvaal Craton (South Africa): revealing multiple events of dyke emplacement. (45 hp)
458. Zaman, Patrik, 2015: LiDAR mapping of presumed rock-cored drumlins in the Lake Åsnen area, Småland, South Sweden. (15 hp)
459. Aguilera Pradenas, Ariam, 2015: The formation mechanisms of Polycrystalline diamonds: diamondites and carbonados. (15 hp)
460. Viehweger, Bernhard, 2015: Sources and effects of short-term environmental changes in Gullmar Fjord, Sweden, inferred from the composition of sedimentary organic matter. (45 hp)
461. Bokhari Friberg, Yasmin, 2015: The paleoceanography of Kattegat during the last deglaciation from benthic foraminiferal stable isotopes. (45 hp)
462. Lundberg, Frans, 2016: Cambrian stratigraphy and depositional dynamics based on the Tomten-1 drill core, Falbygden, Västergötland, Sweden. (45 hp)
463. Flindt, Anne-Cécile, 2016: A pre-LGM sandur deposit at Fiskarheden, NW Dalarna - sedimentology and glaciotectonic deformation. (45 hp)
464. Karlatou-Charalampopoulou, Artemis, 2016: Vegetation responses to Late Glacial climate shifts as reflected in a high resolution pollen record from Blekinge, south-eastern Sweden, compared with responses of other climate proxies. (45 hp)
465. Hajny, Casandra, 2016: Sedimentological study of the Jurassic and Cretaceous sequence in the Revinge-1 core, Scania. (45 hp)
466. Linders, Wictor, 2016: U-Pb geochronology and geochemistry of host rocks to the Bastnäs-type REE mineralization in the Riddarhyttan area, west central Berglsagen, Sweden. (45 hp)
467. Olsson, Andreas, 2016: Metamorphic record of monazite in aluminous migmatitic gneisses at Stensjöstrand, Sveconorwegian orogen. (45 hp)
468. 468. Liesirova, Tina, 2016: Oxygen and its impact on nitrification rates in aquatic

sediments. (15 hp)

469. Perneby Molin, Susanna, 2016: Embryologi och tidig ontogeni hos mesozoiska fisködlor (Ichthyopterygia). (15 hp)
470. Benavides Höglund, Nikolas, 2016: Digitization and interpretation of vintage 2D seismic reflection data from Hanö Bay, Sweden. (15 hp)
471. Malmgren, Johan, 2016: De mellankambriska oelandicuslagren på Öland - stratigrafi och faciestyper. (15 hp)
472. Fouskopoulos Larsson, Anna, 2016: XRF -studie av sedimentära borrkärnor - en metodikstudie av programvarorna Q-spec och Tray-sum. (15 hp)
473. Jansson, Robin, 2016: Är ERT och Tidsdomän IP potentiella karteringsverktyg inom miljögeologi? (15 hp)
474. Heger, Katja, 2016: Makrofossilanalys av sediment från det tidig-holocena undervattenslandskapet vid Haväng, östra Skåne. (15 hp)
475. Swierz, Pia, 2016: Utvärdering av vattenkemisk data från Borgholm kommun och dess relation till geologiska förhållanden och markanvändning. (15 hp)
476. Mårdh, Joakim, 2016: WalkTEM-undersökning vid Revingehed provpumpningsanläggning. (15 hp)
477. Rydberg, Elaine, 2016: Gummigranulat - En litteraturstudie över miljö- och hälsopåverkan vid användandet av gummigranulat. (15 hp)
478. Björnfors, Mark, 2016: Kusterosion och äldre kustdyners morfologi i Skälderviken. (15 hp)
479. Ringholm, Martin, 2016: Klimatutlöst matbrist i tidiga medeltida Europa, en jämförande studie mellan historiska dokument och paleoklimatarkiv. (15 hp)
480. Teilmann, Kim, 2016: Paleomagnetic dating of a mysterious lake record from the Kerguelen archipelago by matching to paleomagnetic field models. (15 hp)
481. Schönström, Jonas, 2016: Resistivitets- och markradarmätning i Ängelholmsområdet - undersökning av korrosiva markstrukturer kring vattenledningar. (15 hp)
482. Martell, Josefin, 2016: A study of shock-metamorphic features in zircon from the Siljan impact structure, Sweden. (15 hp)
483. Rosvall, Markus, 2016: Spår av himlakroppskollisioner - bergarter i nedslagskratrar med fokus på Mien, Småland. (15 hp)
484. Olausson, My, 2016: Resistivitets- och IP -mätningar på den nedlagda deponin Gustavsfält i Halmstad. (30 hp)
485. Plan, Anders, 2016: Markradar- och resistivitetsmätningar – undersökningar utav korrosionsförhöjande markegenskaper kring fjärrvärmeledningar i Ängelholm. (15 hp)
486. Jennerheim, Jessica, 2016: Evaluation of methods to characterise the geochemistry of limestone and its fracturing in connection to heating. (45 hp)
487. Olsson, Pontus, 2016: Ekologiskt vatten från Lilla Klåveröd: en riskinventering för skydd av grundvatten. (15 hp)
488. Henriksson, Oskar, 2016: The Dynamics of Beryllium 10 transport and deposition in lake sediments. (15 hp)
489. Brådenmark, Niklas, 2016: Lower to Middle Ordovician carbonate sedimentology and stratigraphy of the Pakri peninsula, north-western Estonia. (45 hp)
490. Karlsson, Michelle, 2016: Utvärdering av metoderna DCIP och CSIA för identifiering av nedbrytningszoner för klorerade lösningsmedel: En studie av Färgaren 3 i Kristianstad. (45 hp)
491. Elali, Mohammed, 2016: Flygsanddyners inre uppbyggnad – georadarundersökning. (15 hp)
492. Preis-Bergdahl, Daniel, 2016: Evaluation of DC Resistivity and Time-Domain IP Tomography for Bedrock Characterisation at Önneslöv, Southern Sweden. (45 hp)

LUNDS UNIVERSITET

Geologiska institutionen
Lunds universitet
Sölvegatan 12, 223 62 Lund